

# Two-sample Statistics Based on Anisotropic Kernels

Xiuyuan Cheng<sup>\*1</sup>, Alexander Cloninger<sup>\*2</sup>, and Ronald R. Coifman<sup>3</sup>

<sup>1</sup>Department of Mathematics, Duke University

<sup>2</sup>Department of Mathematics, University of California, San Diego

<sup>3</sup>Department of Mathematics, Yale University

## Abstract

The paper introduces a new kernel-based Maximum Mean Discrepancy (MMD) statistic for measuring the distance between two distributions given finitely-many multivariate samples. When the distributions are locally low-dimensional, the proposed test can be made more powerful to distinguish certain alternatives by incorporating local covariance matrices and constructing an anisotropic kernel. The kernel matrix is asymmetric; it computes the affinity between  $n$  data points and a set of  $n_R$  reference points, where  $n_R$  can be drastically smaller than  $n$ . While the proposed statistic can be viewed as a special class of Reproducing Kernel Hilbert Space MMD, the consistency of the test is proved, under mild assumptions of the kernel, as long as  $\|p - q\| \sim O(n^{-1/2+\delta})$  for any  $\delta > 0$ , based on a result of convergence in distribution of the test statistic. Applications to flow cytometry and diffusion MRI datasets are demonstrated, which motivate the proposed approach to compare distributions.

## 1 Introduction

We address the problem of comparing two probability distributions  $p$  and  $q$  from finite samples in  $\mathbb{R}^d$ , where both distributions are assumed to be continuous (with respect to Lebesgue measure) and compactly supported. We consider the case where each distribution is observed from i.i.d. samples, called  $X (\sim p)$  and  $Y (\sim q)$  respectively, and the two datasets  $X$  and  $Y$  are independent. The methodology has applications in a variety of fields, particularly in bio-informatics. It can be used, for example, to test genetic similarities between subtypes of cancers, to compare patient groups to determine potential treatment propensity, and to detect small anomalies in medical images that are symptomatic of a certain disease. We will cover applications to flow cytometry and diffusion MRI data sets in this paper.

Due to the complicated nature of the datasets we would like to study, we are interested in the general alternative hypothesis test  $\mathcal{H}_0 : p = q$  against  $\mathcal{H}_1 : p \neq q$ . This goes beyond tests of possible shifts of finite moments, for example, that of mean-shift alternatives namely  $\mathbb{E}_{X \sim p}[X] \stackrel{?}{=} \mathbb{E}_{Y \sim q}[Y]$ . We also focus on

---

<sup>\*</sup>The majority of this work was done while the first two authors were Gibbs Assistant Professors at Yale.

the medium dimensional setting, in which  $1 < d \ll \min(n_1, n_2)$ , where  $n_1$  ( $n_2$ ) is the number of samples in  $X$  ( $Y$ ). As  $n \rightarrow \infty$ , the dimension  $d$  is assumed to be fixed. (For the scenario where  $d \sim O(n)$ , the convergence of kernel matrices to the limiting integral operator needs to be treated quite differently, and a new analysis is needed.) We are particularly interested in the situation where data is sampled from distributions which are locally low-rank, which means that the local covariance matrices are generally of rank much smaller than  $d$ . As will be clear in the analysis, the approach of constructing anisotropic kernels is most useful when data exhibits such characteristics in a high dimensional ambient space.

We are similarly concerned with a  $k$ -sample problem, in which the question is to determine the global relationships between  $k$  distributions, each of which has a finite set of i.i.d. samples. This can be done by measuring a pairwise distance between any two distributions and combining these pairwise measurements to build a weighted graph between the  $k$  distributions. Thus we focus on the two-sample test as the primary problem.

In the two-sample problem, the two data sets do not have any point-to-point correspondence, which means that they need to be compared in terms of their probability densities. One way to do this is to construct “bins” at many places in the domain, compute the histograms of the two datasets at these bins, and then compare the histograms. This turns out to be a good description of our basic strategy, and the techniques beyond this include using “anisotropic gaussian” bins at every local point and “smoothing” the histograms when needed. Notice that there is a trade-off in constructing these bins: if a bin is too small, which may leave no points in it most of the time, the histogram will have a large variance compared to its mean. When a bin is too large, it will lose the power to distinguish  $p$  and  $q$  when they only differ slightly within the bin. In more than one dimension, one may hope to construct anisotropic bins which are large in some directions and small in others, so as maximize the power to differentiate  $p$  and  $q$  while maintaining small variance. It turns out to be possible when the deviation ( $q - p$ ) has certain preferred (local) directions. We illustrate this idea in a toy example below, and the analysis of testing consistency, including the comparison of different “binning” strategies, is carried out by analyzing the spectrum of the associated kernels in Section 3.

At the same time, we are not just interested in whether  $p$  and  $q$  deviate, but how and where they deviate. The difference of the histograms of  $X$  and  $Y$  measured at multiple bins, introduced as above, can surely be used as an indication of where  $p$  and  $q$  differ. The formal concept is known as the *witness function* in literature, which we introduce in Section 2.3 and use throughout the applications.

The idea of using bins and comparing histograms dates back to measuring distribution distances based on kernel density estimation, and is also closely related to two-sample statistics by Reproducing Kernel Hilbert Space (RKHS) Maximum-mean discrepancy (MMD). We discuss these connections in more detail in Section 1.2. While anisotropic kernels have been previously studied in manifold learning and image processing, kernel-based two-sample statistics with anisotropic kernels have not been examined in the situation where the data is locally low-rank, which is the theme of the current paper.

This paper yields several contributions to the two sample problem. Methodologically, we introduce a kernel-based MMD statistic that increases the testing power against certain deviated distributions by adopting an

anisotropic kernel, and reduces both the computation and memory requirements. The proposed method can be combined with spectral smoothing of the histograms in order to reduce variability and possibly optimize the importance of certain regions of data, so that the power of the test maybe furtherly improved. Theoretically, asymptotic consistency is proved for any fixed deviation beyond the critical regime  $\|p - q\| \sim O(n^{-1/2})$  under generic assumptions. Experimentally, we provide two novel applications of two-sample and  $k$ -sample problems for biological datasets.

The rest of the paper is organized as follows: we begin with a sketch of the main idea and motivating example in the remainder of this section, together with a review of previous studies. Section 2 formalizes the definition of the MMD statistics being proposed. Asymptotic analysis is given in Section 3. The algorithm and other implementation matters, including computation complexity, are discussed in Section 4. Section 5 covers numerical experiments on synthetic and real-world datasets.

## 1.1 Main Idea

Let  $p$  and  $q$  be two distributions supported on a compact set  $\Omega \subset \mathbb{R}^d$ . Suppose that a reference set  $R$  is given, and for each point  $r \in R$  there is a (non-degenerate) covariance matrix  $\Sigma_r$  (e.g. computed by local PCA). We define the asymmetric affinity kernel to be

$$a(r, x) = e^{-\|r-x\|_{\Sigma_r}^2} = \exp\left\{-\frac{1}{2}(x-r)^T \Sigma_r^{-1}(x-r)\right\}, \quad \forall r \in R, x \in \Omega. \quad (1)$$

Consider the two independent datasets  $X \sim p$  and  $Y \sim q$ , where  $X$  has  $n_1$  i.i.d. samples and  $Y$  has  $n_2$  i.i.d. samples. The empirical histograms of  $X$  and  $Y$  at the reference point  $r$  are defined as

$$\hat{h}_X(r) = \frac{1}{n_1} \sum_{i=1}^{n_1} a(r, X_i), \quad \hat{h}_Y(r) = \frac{1}{n_2} \sum_{j=1}^{n_2} a(r, Y_j), \quad (2)$$

for which the population quantities are

$$h_p(r) = \int a(r, x)p(x)dx, \quad h_q(r) = \int a(r, y)q(y)dy. \quad (3)$$

The empirical histograms are nothing else but the Gaussian binning of  $X$  and  $Y$  at point  $r$  with the anisotropic bins corresponding to the covariance matrix  $\Sigma_r$ . We then compute the quantity

$$T = \frac{1}{n_R} \sum_{r \in R} (\hat{h}_X(r) - \hat{h}_Y(r))^2 \quad (4)$$

as a measurement of the (squared) distance between the two datasets.

We use the following example to illustrate the difference between (1) using anisotropic kernel where  $\Sigma_r$  is aligned with the tangent space of the manifold data, and (2) using the isotropic ones where  $\Sigma_r$  is a multiple of the identity matrix.

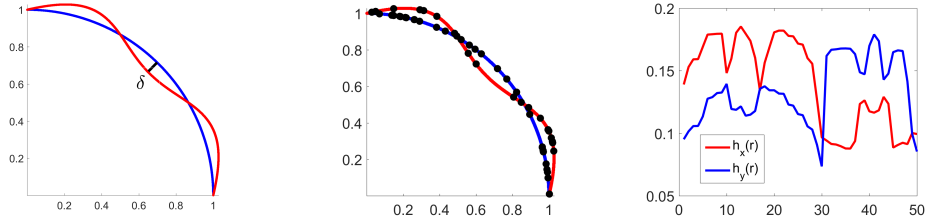


Figure 1: (Left)  $X$  and  $Y$  sampled from curves in  $\mathbb{R}^2$  with separation of  $\delta = 0.05$ . (Middle) Location of 50 reference points sampled from data. (Right) Values of  $\hat{h}_X(r)$  and  $\hat{h}_Y(r)$  across reference points, computed from the anisotropic kernel.

The data is like in Figure 1, where  $p$  and  $q$  are supported on two arcs in  $\mathbb{R}^2$  separated by a gap of size  $\delta$  at various regions. We begin by specifying a reference set  $R$  and the covariance field  $\{\Sigma_r\}_{r \in R}$ . For simplicity, we do this by uniformly sampling  $n_R = 50$  reference points from  $X \cup Y$  (middle of Figure 1). At each reference point  $r$ , we take  $k = 50$  neighbors  $\{x_{i,j}\}_{j=1}^k$  to estimate the local covariance matrix by  $\Sigma_r = \frac{1}{k} \sum_{i=1}^k (x_{j_i} - r)(x_{j_i} - r)^T$ . The empirical histograms  $\hat{h}_X(r)$  and  $\hat{h}_Y(r)$  are computed as in Eqn. (2) at every point  $r$  (right of Figure 1), as well as the quantity  $T$  as in Eqn. (4). We also compute  $T$  under a permutation of the data points in  $X$  and  $Y$  so as to mimic the null hypothesis  $p = q$ , and we call the two values  $T_1$  and  $T_0$  respectively. The experiment is repeated 100 times, where  $n_1 = n_2 = 2000$ , and the distribution of  $T_1$  and  $T_0$  are shown as red and blue bars in Figure 2. The simulation is done across three datasets where  $\delta$  takes value as  $\{0, 0.01, 0.05\}$ , and we compare isotropic and anisotropic kernels. When  $\delta = 0$ , the distributions of  $T_0$  and  $T_1$  overlay each other, as expected. When  $\delta > 0$ , greater separation between distributions of  $T_0$  and  $T_1$  implies greater power for the test. The advantage of the anisotropic kernel is clearly demonstrated, particularly when  $\delta = 0.01$  (the middle row).

The analysis of the testing power of  $T$  hinges on the singular value decomposition of  $a(r, x)$ , formally written as  $a(r, x) = \sum_k \sigma_k \phi_k(r) \psi_k(x)$  and will be defined in Section 3. The histogram  $\hat{h}_X(r)$  thus becomes  $\sum_k \sigma_k \phi_k(r) \left( \frac{1}{n_1} \sum_i \psi_k(x_i) \right)$ , and similarly for  $\hat{h}_Y(r)$ , which means that the ability of  $T$  to distinguish  $p$  and  $q$  is determined by the amount that  $X$  and  $Y$  differ when projected onto the singular functions  $\psi_k$ . For the example above, the first few singular functions are visualized in Figure 3, where the  $\psi_k$ 's of the anisotropic kernel project along the directions where  $q$  and  $p$  deviate at a lower index of  $k$ , thus contributing more significantly to the quantity  $T$ . Figure 3 also shows the witness function of the kernels, which combines the singular vectors to show there regions of deviation between  $p$  and  $q$ .

For clarification throughout the paper, we refer to the use of a local Mahalanobis distance with  $\Sigma_r \neq I$  as an anisotropic kernel and  $\Sigma_r = c \cdot I$  as an isotropic kernel. Similarly, we refer to a kernel measuring affinity from all points to a reference set (i.e.  $\mathbb{R}^d \times \Omega \rightarrow \mathbb{R}$ ) as an asymmetric kernel. The analysis in Section 3 is for the symmetrized version of the kernel  $k(x, y) = \int a(r, x) a(r, y) d\mu_R(r)$ , while in practice one never computes the  $n$ -by- $n$  kernel but only the  $n_R$ -by- $n$  asymmetric kernel  $a(r, x)$  which is equivalent and way more efficient. We discuss more about computation in Section 4.4.

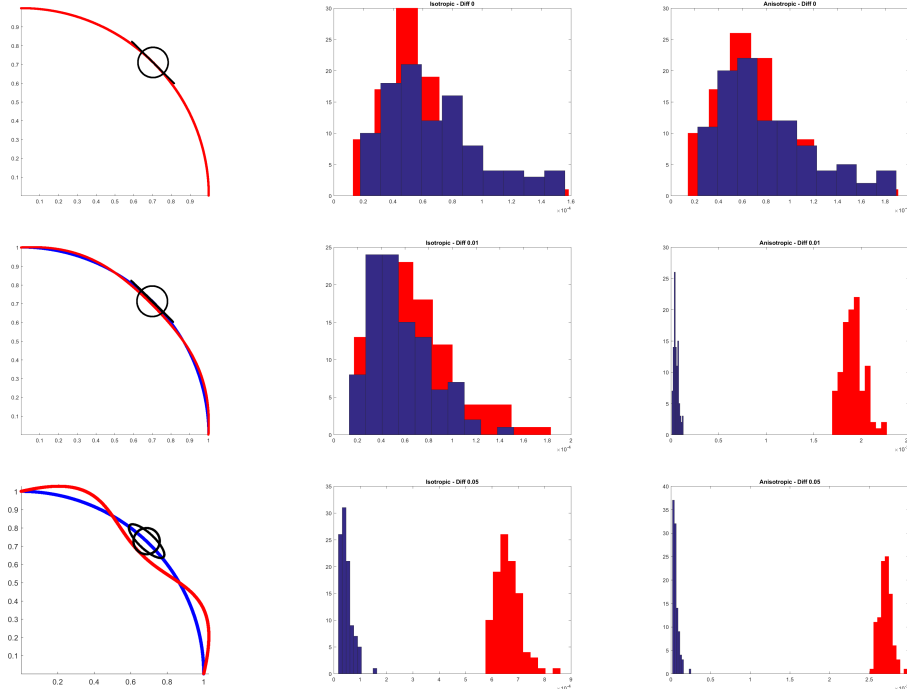


Figure 2: Distribution of the distance measurement  $T$  in Eqn. (4) using isotropic and anisotropic kernels, top:  $\delta = 0$ , middle:  $\delta = 0.01$ , bottom:  $\delta = 0.05$ . (Left) two data sets with representative isotropic and anisotropic bins. (Middle) histograms of  $T_0$  (in blue) and  $T_1$  (in red) when using isotropic kernel. (Right) histograms of  $T_0$  and  $T_1$  when using anisotropic kernel.

## 1.2 Related Work

The question of two sample testing is a central problem in statistics. In one dimension, one classical approach to two sample testing is the Kolmogorov-Smirnov distance, which compares the  $L^\infty$  distance between the two empirical cumulative distribution functions [16, 24]. While there exist generalizations of these infinitely supported bins in high dimensions [4, 11, 21, 13], these require a large computational cost for either computing a minimum spanning tree or running a large number of randomized tests. This warranted binning functions that are defined more locally and in a data-adaptive fashion. Another high-dimensional extension of Kolmogorov-Smirnov is to randomly project the data into a low-dimensional space and compute the test in each dimension.

The 1D Kolmogorov-Smirnov statistic can be seen as a special case of the MMD discrepancy, which is generally defined as

$$\text{MMD}(p, q; \mathcal{F}) = \sup_{f \in \mathcal{F}} \int f(x)(p(x) - q(x))dx,$$

where  $\mathcal{F}$  is certain family of integrable functions. When  $\mathcal{F}$  equals the set of all indicator functions of intervals  $(-\infty, t)$  in  $\mathbb{R}$ , the MMD discrepancy gives the Kolmogorov-Smirnov distance. Kernel-based MMD has been studied in [12], where the function class  $\mathcal{F}$  consists of all functions s.t.  $\|f\|_{\mathcal{H}} \leq 1$ , where

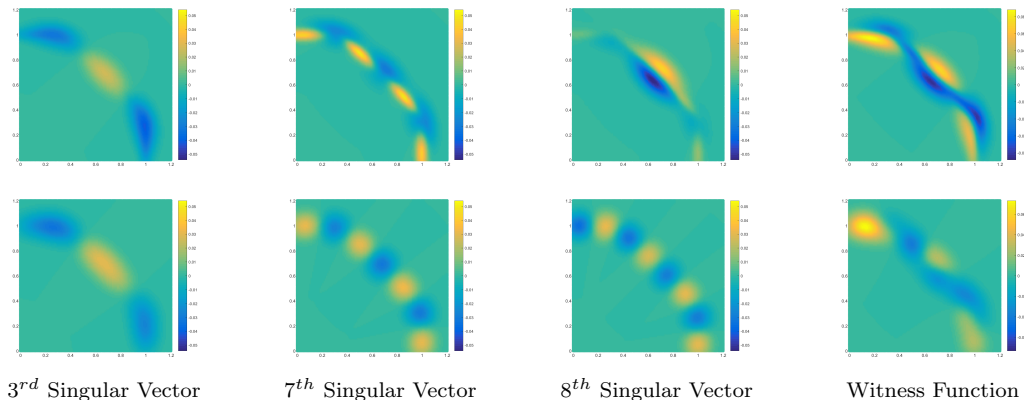


Figure 3: The colorfield visualizes  $\psi_k$  as singular functions of  $a(r, x)$ ,  $k = 3, 7, 8$ , for the example in Figure 1 with  $\delta = 0.05$ . (Top)  $\psi_k$  of anisotropic kernel. (Bottom)  $\psi_k$  of isotropic kernel. The  $\psi_k$ 's of the two kernels more or less agree up to  $k \leq 6$ . The right column visualizes the witness function of each kernel, using only  $n_1 = n_2 = 500$  points sampled from  $p$  and  $q$ .

$\|\cdot\|_{\mathcal{H}}$  indicates the norm of the Hilbert space associated with the reproducing kernel. Specifically, suppose the PSD kernel is  $k(x, y)$ , the (squared) RKHS MMD can be written as

$$\text{MMD}^2(p, q) = \int \int k(x, y)(p(x) - q(x))(p(y) - q(y))dxdy, \quad (5)$$

and can be estimated by (here we refer to the biased estimator in [12] which includes the diagonal terms)

$$\text{MMD}^2(X, Y) = \frac{1}{n_1^2} \sum_{x, x' \in X} k(x, x') + \frac{1}{n_2^2} \sum_{y, y' \in Y} k(y, y') - \frac{2}{n_1 n_2} \sum_{x \in X, y \in Y} k(x, y).$$

The methodology and theory apply to any dimensional data as long as the kernel can be evaluated.

We consider a kernel  $k(x, y)$  of the form  $k(x, y) = \int a(r, x)a(r, y)d\mu_R(r)$  and its variants, where  $d\mu_R$  is certain measure of the reference points. This can be seen as a special case of RKHS MMD [12], which considers a general PSD kernel  $k : X \times X \rightarrow \mathbb{R}^+$ . When  $a(r, x) = a(r - x)$  and is isotropic,  $d\mu_R$  is the Lebesgue measure,  $k(x, y)$  is reduced to gaussian kernel. However, returning to the asymmetric kernel as we do, allows us to easily redefine the local geometry around reference points and incorporate the local dimensionality reduction in (1). While the asymmetric kernel requires the additional slight assumption that the eigenmodes of the kernel do not vanish on the support of  $p$  and  $q$ , which is discussed in Gretton [12] in reference to isotropic Parzen windows, this yields a more powerful test for distributions that are concentrated near locally low-dimensional structures. In terms of analysis, our theory gives a quantitative comparison of the testing powers of different kernels, which turns out to be determined by the spectral decomposition of the kernels. This analysis augments the analysis of [12]; the asymptotic distribution results in [12] does not imply testing power in high dimensions, as pointed out later by [20]. Our analysis borrows techniques from that of the classical V-statistic [22], and it makes use of the spectral decomposition

of the kernel with respect to the data distribution. While the empirical spectral expansion of translation-invariant kernels has been previously used to derive two-sample statistics, e.g. in [10] and more recently in [7, 26], and the idea dates back to earlier statistical works (see e.g. [9]), our setting is different due to the new construction of the kernel.

Our approach is also closely related to the previous study of the distribution distance based on kernel density estimation [1]. We generalize the results in [1] by considering non-translation-invariant kernels, which greatly increases the separation between the expectation of  $T_n$  under the null hypothesis and the expectation of  $T_n$  under an alternative hypothesis. Moreover, it is well-known that kernel density estimation, which [1] is based on, converges poorly in high dimension. In the manifold setting, the problem was remedied by normalizing the (isometric) kernel in a modified way and the estimation accuracy was shown to only depend on the intrinsic dimension [19]. Our proposed approach takes extra advantage of the locally low dimensional structure, and obtains improved distinguishing power compared to the one using isotropic kernels when possible.

At last, the proposed approach can be viewed as related to two sample testing via nearest neighbors [14]. In [14], one computes the nearest neighbors of a reference point  $r$  to the data  $X \cup Y$  and derives a statistical test based on the amount the empirical ratio  $\frac{k_X}{k_X+k_Y}$ , where  $k_X$  is the number of neighbors from  $X$  (similarly  $k_Y$ ), deviates from the expected ratio under the null hypothesis, namely  $\frac{n_1}{n_1+n_2}$ . Because the nearest neighbor algorithm is based on Euclidean distance, it is equivalent to a kernel-based MMD with a hard-thresholded isotropic kernel. The approach can be similarly combined with a local Mahalanobis distance as we do, which has not been explored.

## 2 Test Statistics and Witness Functions

We recall the setting up of the problem: given two independent datasets  $X$  and  $Y$ , where  $X$  has  $n_1$  i.i.d. samples drawn from distribution  $p$ , and  $Y$  has  $n_2$  i.i.d. samples drawn from  $q$ .  $p$  and  $q$  are supported on compact subset of  $\mathbb{R}^d$ . We also assume that  $p$  and  $q$  has continuous probability density, so we interchange the notation  $dp$  and  $p(x)dx$  and similarly for  $dq$ . In this section and next, we assume that the covariance field  $\{\Sigma_r\}_r$ , which is needed to compute  $a(r, x)$ , is pre-defined.

Our goal is two-folded: (i) to test the hypothesis  $p = q$  against the alternative, and (ii) in case that  $q \neq p$ , to derive certain estimators which can detect where the two distributions differ. We will introduce certain RKHS MMD statistics for (i), which also give the witness function for the purpose of (ii).

### 2.1 Kernel MMD statistics

Using the kernel  $a(r, x)$  defined in Eqn. (1), we consider the following empirical statistic:

$$\hat{T}_{L^2} = \int |\hat{h}_X(r) - \hat{h}_Y(r)|^2 d\mu_R(r), \tag{6}$$

where  $\hat{h}_X(r)$  and  $\hat{h}_Y(r)$  are defined in Eqn. (2). The above definition assumes the measure  $\mu_R$  which is a distribution of the reference point.  $\mu_R$  can be any distribution in general, and in practice, it is an empirical distribution over the finite set  $R$ , i.e.  $d\mu_R = \frac{1}{n_R} \sum_{r \in R} \delta_r$ , where  $n_R$  is the number of points in  $R$ . For now we leave  $\mu_R$  to be general. The population statistic corresponding to Eqn. (6) is  $T_{L^2} = \int |h_p(r) - h_q(r)|^2 d\mu_R(r)$ . We consider a more general construction as

$$T_{\text{general}} = \int \int L(r, r') (h_p(r) - h_q(r)) (h_p(r') - h_q(r')) d\mu_R(r) d\mu_R(r') \quad (7)$$

where  $L(r, r')$  is a PSD kernel.  $T_{\text{general}}$  reduces to  $T_{L^2}$  when  $L(r, r') = \delta(r - r')$ . The involvement of  $L(r, r')$  has several motivations: it allows to include a (positive) weight on reference point  $r$  if needed, in which case  $L(r, r') = w(r)\delta(r - r')$ ; another motivation is spectral filtering on manifolds, which will be further explained below.

The above statistics can be viewed as special forms of RKHS MMD: according to Eqn. (5), Eqn. (7) is nothing but the (squared) RKHS MMD with the kernel

$$k(x, y) = \int L(r, r') a(r, x) a(r', y) d\mu_R(r) d\mu_R(r'), \quad (8)$$

and for  $T_{L^2}$  it is reduced to

$$k_{L^2}(x, y) = \int a(r, x) a(r, y) d\mu_R(r). \quad (9)$$

The kernel (9), and generally (8), is positive definite, however, not necessarily “universal”, means that the population MMD as in Eqn. (7) being zero does not guarantee that  $q = p$ . In other words, the reproducing kernel Hilbert space associated with  $k(x, y)$  does not include all distributions. The test is thus restricted to the departures within the Hilbert space (Assumption 2). We sacrifice the universal property of the kernel to obtain potentially stronger power when the departure is indeed in the Hilbert space.

## 2.2 Spectral filtering by $L(r, r')$

The reference set is sampled at region where  $p$  and  $q$  are supported. When the distributions  $p$ ,  $q$  and  $\mu_R$  are all centered around certain manifold, and  $p$  and  $q$  are smooth with respect to the manifold, one would expect the histograms  $\hat{h}_X$  and  $\hat{h}_Y$  to be smooth as well. This suggests to filter the two histograms before computing the  $L^2$  distance between the two length- $n_R$  vectors.

To be specific, let  $d\mu(x)$  be the distribution which is a mixture of  $p$  and  $q$  to be specified later, since  $a(r, x)$  is bounded by 1, so is the integral  $\int \int a(r, x)^2 d\mu_R(r) d\mu(x)$ , and thus the asymmetric kernel is Hilbert-Schmidt and the integral operator is compact. The singular value decomposition of  $a(r, x)$  with respect to  $d\mu_R$  and  $d\mu$  can be written as

$$a(r, x) = \sum_k \sigma_k \phi_k(r) \psi_k(x),$$

where  $\sigma_k > 0$ ,  $\{\phi_k\}_k$  and  $\{\psi_k\}$  are ortho-normal sets w.r.t  $d\mu_R(r)$  and  $d\mu(x)$  respectively, and the kernel

in Eqn. (9) can be written as

$$k_{L^2}(x, y) = \sum_k \sigma_k^2 \psi_k(x) \psi_k(y). \quad (10)$$

One can modify the kernel to be

$$k_{\text{spec}}(x, y) = \sum_k f_k \psi_k(x) \psi_k(y) \quad (11)$$

where  $f_k$  is a sequence of sufficiently decaying positive numbers, which is equivalent to setting  $L(r, r') = \sum_k \frac{f_k}{\sigma_k^2} \phi_k(r) \phi_k(r')$  whenever the sequence is summable. This leads to the following statistic

$$T_{\text{spec}} = \sum_k f_k \left( \int (h_p(r) - h_q(r)) \phi_k(r) d\mu_R(r) \right)^2. \quad (12)$$

The assumptions on  $f_k$  will be clear in the analysis. In practice, the SVD is approximated by that of the matrix of size  $n_R$ -by- $(n_1 + n_2)$  consisting of values  $a(r, x_i)$  and  $a(r, y_j)$ , which means that  $d\mu$  is  $\frac{n_1}{n_1+n_2} dp + \frac{n_2}{n_1+n_2} dq$ . In the empirical version of Eqn. (12), the singular functions  $\phi_k(r)$  is approximated by empirical singular vectors, apart from that the histograms are replaced by empirical counterparts.

For the purpose of smoothing histograms, one can assign small values of  $f_k$  for large  $k$ , which means that high-frequency components of the histograms are less weighted. If prior knowledge about the magnitude of projection  $\int (p(x) - q(x)) \psi_k(x) d\mu(x)$  is available, one may also choose  $f_k$  accordingly. The construction Eqn. (11) is quite flexible, for example, setting  $f_k = \sigma_k^{2(m+1)}$  is equivalent to letting  $L(r, r')$  be  $m$  “powers” of the kernel  $\int a(r, x) a(r', x) d\mu(x)$  on the space of  $r$ , which filters high frequency modes. This extension of kernel MMD may be of interest even when  $a(r, x)$  is the isotropic gaussian kernel.

Further more, one may view the data sets  $\tilde{X}$ , consisting of  $\tilde{x}_i = \{\psi_k(x_i)\}_{1 \leq k \leq K}$ , and  $\tilde{Y}$ , consisting of  $\tilde{y}_j = \{\psi_k(x_j)\}_{1 \leq k \leq K}$ , as another two samples in  $\mathbb{R}^K$ , which have  $K$  uncorrelated coordinates (w.r.t the mixed density) thanks to the orthogonality of  $\psi_k$ . We will further comment on this point of view in Section 6, while the paper is mainly concerned with the statistics  $T_{L^2}$  and  $T_{\text{spec}}$ .

### 2.3 Witness functions

Following the convection in RKHS MMD, the witness function  $w(x)$  is defined as the maximizer of

$$\max_{w \in \mathcal{H}, \|w\|_{\mathcal{H}}=1} \langle w, \mu_p - \mu_q \rangle_{\mathcal{H}}$$

where  $\mu_p$  and  $\mu_q$  are the mean embedding of  $p$  and  $q$  in  $\mathcal{H}$  respectively. By Riez representation,  $w$  equals  $(\mu_p - \mu_q)$  multiplied by a constant. We will thus consider  $w = \mu_p - \mu_q$  as the witness function. By definition,  $\mu_p(x) = \int k(x, y) p(y) dy$ , and similarly for  $\mu_q$ , thus  $w(x) = \int k(x, y) (p(y) - q(y)) dy$ .

Inserting Eqn. (8) we obtain that for the general statistic  $T_{\text{general}}$ ,

$$w(x) = \int L(r, r') a(r, x) (h_p(r') - h_q(r')) d\mu_R(r) d\mu_R(r'),$$

and particularly for  $T_{L^2}$ ,

$$w_{L^2}(x) = \int a(r, x) (h_p(r) - h_q(r)) d\mu_R(r). \quad (13)$$

For  $T_{\text{spec}}$ ,

$$w_{\text{spec}}(x) = \sum_k f_k \psi_k(x) \int \psi_k(y) (p(y) - q(y)) dy. \quad (14)$$

The computation of the witness function will be discussed in Section 4.2

Although witness function is not an estimator of the difference of the density  $(p - q)$ , it gives a function of where  $q$  and  $p$  deviate most, and thus can be very useful for user interpretation of the two sample test, as shown in several examples in Section 5. Particularly, the witness function can indicate local discrepancies of  $q - p$ , beyond the MMD statistics which is a global quantity.

### 3 Asymptotic Analysis and Testing Power

To unifying the analysis of  $T_{L^2}$  and  $T_{\text{spec}}$ , we consider the RKHS MMD (population) statistic  $T$  of the following form

$$T(p, q) = \int \int k(x, y) (p(x) - q(x)) (p(y) - q(y)) dx dy, \quad (15)$$

where  $k(x, y)$  is a positive definite kernel. The empirical version is

$$T_n(X, Y) = \int \int k(x, y) (\hat{p}_X(x) - \hat{q}_Y(x)) (\hat{p}_X(y) - \hat{q}_Y(y)) dx dy, \quad (16)$$

where  $\hat{p}_X = \frac{1}{n_1} \sum_i \delta_{x_i}$  and  $\hat{q}_Y = \frac{1}{n_2} \sum_j \delta_{y_j}$ , and  $n = n_1 + n_2$ . We consider the limit where both  $n_1$  and  $n_2$  go to infinity and proportional to each other, in other words,  $n \rightarrow \infty$  and  $\frac{n_1}{n} \rightarrow \rho_1 \in (0, 1)$ , and  $\frac{n_2}{n} \rightarrow \rho_2 = 1 - \rho_1$ , so we denote the statistic by subscript  $n$ . The empirical statistic  $T_n$  has the aforementioned forms as  $\hat{T}_{L^2}$  and  $\hat{T}_{\text{spec}}$  when  $k(x, y)$  is set to be  $k_{L^2}$  and  $k_{\text{spec}}$  respectively.

The power of the test is dictated by the distribution of  $T_n(X, Y)$  under  $\mathcal{H}_0 : p = q$  and  $\mathcal{H}_1 : p \neq q$ . We will specify the family of alternative  $q$  that can be distinguished in [Assumption 2]. The power is defined in the following way: let  $t_\alpha$  be the  $\alpha$ -level threshold of  $T_n$  under  $\mathcal{H}_0$ , that is

$$\Pr[T_n > t_\alpha | \mathcal{H}_0] = \alpha, \quad (17)$$

and we reject  $\mathcal{H}_0$  whenever  $T_n > t_\alpha$ . The power of the test (with finite sample) against an alternative  $q$  is defined as

$$\pi_n(q) = \Pr[T_n > t_\alpha | \mathcal{H}_1 \text{ with } q],$$

and the test is consistent if  $\pi_n(q) \rightarrow 1$  as  $n \rightarrow \infty$ . We will show that, as long as  $\int a(r, x)(p(x) - q(x))dx$  as a function does not vanish, the test based on  $T_n$  is consistent. The asymptotic consistency still holds when allowing  $q$  to depend on  $n$  in the way as  $q_n = p + \tau_n(q_1 - p)$  where  $\tau_n$  decreases to 0 slower than  $n^{-1/2}$ . The analysis also leads to a quantitative comparison of different kernels in terms of testing power.

### 3.1 Assumptions of the kernel

Due to that  $a(r, x)$  is uniformly bounded and Hilbert-Schmidt,  $k_{L^2}(x, y)$  is PSD, Hilbert-Schmidt thus compact, and then can be expanded as in Eqn. (10) where  $\{\psi_k\}_k$  are a set of ortho-normal functions under  $\mu = \rho_1 p + \rho_2 q$ . By that  $0 \leq a(r, x) \leq 1$ , we also have that  $k = k_{L^2}$  satisfies that

$$0 \leq k(x, x) \leq 1, \quad \forall x, \quad (18)$$

and  $|k(x, y)| \leq 1$  for any  $(x, y)$ , which can be seen as a consequence of Eqn. (18) as well. Meanwhile,  $k_{L^2}$  is continuous by that  $a(r, x)$  is continuous, which means that the sequence in Eqn. (10) converges uniformly and absolutely, and the eigenfunctions  $\psi_k$  are continuous (Mercer's Theorem). Therefore when modifying the kernel as in Section 2.2, one can preserve the continuity and boundedness of the kernel. At last, Eqn. (18) implies that the operator is in trace class, namely  $\sum_k \lambda_k \leq 1$ .

As has been introduced in Section 2, we analyze kernels of the form

$$k(x, y) = \sum_k f_k \psi_k(x) \psi_k(y), \quad (19)$$

where  $f_k \geq 0$  and  $\sum_k f_k \leq 1$ ,  $\{\psi_k\}_k$  ortho-normal under  $\mu = \rho_1 p + \rho_2 q$ , and we assume that

**Assumption 1.** *The  $f_k$  are chosen so that the kernel  $k(x, y)$  in Eqn. (19) is PSD, continuous, and  $0 \leq k(x, x) \leq 1$ .*

As a result,  $|k(x, y)|$  is uniformly bounded by 1, Mercer Theorem applies to  $k$  so that the spectral expansion Eqn. (19) converges uniformly and absolutely, and the operator is in trace class. Notice that  $k_{L^2}$  is a special case of Eqn. (19) where  $f_k = \sigma_k^2$ , and Assumption 1 is valid. Another example of constructing  $f_k$  is that let  $f_k = \sigma_k^2$  when  $k > k_0$  and  $f_k$  be arbitrary positive numbers when  $k \leq k_0$ , then multiply every  $f_k$  by a global constant to guarantee that  $\sum_k f_k \leq 1$  and  $k(x, x) \leq 1$ .

We now consider what kernel will make  $T(p, q)$  strictly positive when  $q \neq p$ . We have the following

**Proposition 3.1.** *Notations as above, the following are equivalent*

- (i)  $T(p, q) > 0$ ,
  - (ii)  $\int \psi_k(x)(p(x) - q(x))dx \neq 0$  and  $f_k > 0$  for some  $k$ ,
- If  $f_k > 0$  for all  $k$ , then it is equivalent to
- (iii)  $h_p(r) - h_q(r) \neq 0$  a.s. w.r.t  $d\mu_R$ .

*Proof.* By Eqn. (15,19), (i)  $\Leftrightarrow$  (ii). Recall that  $h_p(r) - h_q(r) = \int a(r, x)(p(x) - q(x))dx$ , and that  $a(r, x)$  has the SVD while the right singular functions are  $\psi_k$ , then (iii) is equivalent to  $\int \psi_k(x)(p(x) - q(x))dx \neq 0$  for some  $k$ . When  $f_k$  is all strictly positive, it is equivalent to (ii).  $\square$

Notice that  $k_{L^2}$  satisfies  $f_k > 0$  by definition. The condition that  $f_k$  is always nonzero does not incur any restriction in practice with finite samples, and can be seen as a mathematical convenience.

(iii) of Proposition 3.1 says that the population MMD statistic will be able to distinguish the alternative  $q$  as long as there is some bin at reference  $r$  which distinguish  $p$  and  $q$  by the population histograms. Mathematically speaking, the family of  $q$  which can be distinguished by the MMD are those for which  $(p - q)$  in the subspace spanned by  $\{\psi_k\}_k$  in the Hilbert space with  $d\mu$ . This subspace is usually smaller than the whole space, for example, when the reference set has  $n_R$  points then it is rank at most  $n_R$ . However, when the continuous measure  $d\mu_R$  is smooth, the approximation of the low-frequency eigenfunctions of the kernel  $\int a(r, x)a(r, y)d\mu_R(r)$ , which has a sufficiently decaying spectrum, can be efficiently computed by the right singular functions of  $a(r, x)$  with a drastic down sampling of  $d\mu_R$  [3]. This means that, with finite reference set  $R$ , an alternative  $q$  will makes  $T(p, q) = 0$  only when the departure  $(q - p)$  lies in the high frequency modes. Under certain condition of  $d\mu_R$  (sufficiently overlapping with  $\mu$ ) which we do not further pursue, the assumption that  $\int \psi_k(x)(p(x) - q(x))dx$  does not all vanish turns out to be a mild one for all practical purposes considered in this paper.

We thus introduce the following assumption:

**Assumption 2.** *In Eqn. (19),  $f_k$  are all strictly positive. The alternative  $q \neq p$  satisfies that  $h_p(r) - h_q(r) \neq 0$  a.s. w.r.t  $d\mu_R$ .*

In other words, we consider the family of alternative  $q$  which belongs to

$$\mathcal{Q} = \{q \text{ s.t. } h_p(r) - h_q(r) \neq 0, \text{ a.s. w.r.t. } d\mu_R(r)\},$$

when we always have  $T(p, q) > 0$ .

Assumption 2 can be viewed as a counterpart of the condition of kernel “having non-vanishing Fourier transforms on any interval”, which is needed for the kernel-density-estimation-based  $L^2$  distance (involving translation-invariant kernel) to be a distance (Sec 2.4 [1]). Proposition 3.1 implies that Assumption 1 is equivalent to  $f_k \int \psi_k(x)(p(x) - q(x))dx \neq 0$  for some  $k$ . Viewing  $\psi_k$  as the general Fourier modes, which is the case when  $k(x, y)$  is constructed to approximate certain diffusion kernel on a manifold, then  $T(p, q) > 0$  for any  $q \neq p$  only when the basis  $\{\psi_k, f_k > 0\}$  is complete, namely the kernel has non-vanishing “Fourier transform”.

The discussion so far is about the population statistic  $T$ . With finite samples, apart from having the projection  $\int \psi_k(x)(p(x) - q(x))dx$  non vanishing, we need it to be large enough to overcome the “noise” contributed by finite-sample effect. We address this point in the asymptotic analysis later.

## 3.2 The centered kernel

For convenience of analysis, we consider the centered kernel  $\tilde{k}(x, y)$  under  $p$ , defined as

$$\tilde{k}(x, y) = k(x, y) - k_p(x) - k_p(y) + k_{pp},$$

where  $k_p(x) = \int k(x, y)p(y)dy$ , and  $k_{pp} = \int k_p(x)p(x)dx$ . Notice that the statistic  $T$ , both the population and the empirical version, remains the same if  $k$  is replaced by  $\tilde{k}$ :

**Proposition 3.2.** *Notations as above,*

$$T(p, q) = \int \tilde{k}(x, y)(p(x) - q(x))(p(y) - q(y))dxdy$$

and

$$T_n(X, Y) = \int \int \tilde{k}(x, y)(\hat{p}_X(x) - \hat{q}_Y(x))(\hat{p}_X(y) - \hat{q}_Y(y))dxdy.$$

The proof is by definition and that both  $\int (p(y) - q(y))dy$  and  $\int (\hat{p}_X(y) - \hat{q}_Y(y))dy$  vanish. The kernel  $\tilde{k}$  also inherits the properties of being PSD, bounded and Hilbert-Schmidt from those of  $k$ :

**Proposition 3.3.** *The kernel  $\tilde{k}$ , as an integral operator on the space with the measure  $p(x)dx$ , is PSD. Under Assumption 1,*

(1)  $0 \leq \tilde{k}(x, x) \leq 4$  for any  $x$ , and  $|\tilde{k}(x, y)| \leq 4$  for any  $x, y$ ,

(2)  $\tilde{k}$  is continuous,

(3)  $\tilde{k}$  is Hilbert-Schmidt as an operator on  $L^2(\Omega, p(x)dx)$  and is in the trace class. It has the spectral expansion

$$\tilde{k}(x, y) = \sum_k \tilde{\lambda}_k \tilde{\psi}_k(x) \tilde{\psi}_k(y), \quad (20)$$

where  $\int \tilde{\psi}_k(x)p(x)dx = 0$ ,  $\int \tilde{\psi}_k(x)\tilde{\psi}_l(x)p(x)dx = \delta_{kl}$ ,  $\tilde{\psi}_k$  are continuous on  $\Omega$ ,  $\tilde{\lambda}_k > 0$ ,  $\{\tilde{\lambda}_k\}_k$  are both summable and square summable, and the series in Eqn. (20) converges uniformly and absolutely.

(4) The eigenfunctions  $\tilde{\psi}_k$  are square integrable, and thus integrable, w.r.t.  $q(y)dy$ , and  $\sum_k \tilde{\lambda}_k \int \tilde{\psi}_k(y)^2 q(y)dy$  is finite.

The proof is left to Appendix A. Under Assumption 2,  $T(p, q) > 0$  when  $q \neq p$ . By the spectral expansion Eqn. (20),

$$T(p, q) = \sum_k \tilde{\lambda}_k \left( \int \tilde{\psi}_k(x)(p(x) - q(x))dx \right)^2, \quad \tilde{\lambda}_k > 0,$$

which implies that  $\int \tilde{\psi}_k(x)(p(x) - q(x))dx \neq 0$  for some  $k$ . We thus define

$$\tilde{v}_k := \int \tilde{\psi}_k(x)(p(x) - q(x))dx \quad (21)$$

which vanishes when  $p = q$ . Shortening the notation  $T(p, q)$  as  $T$ ,  $T_n(X, Y)$  as  $T_n$ , we have

$$T = \sum_k \tilde{\lambda}_k \tilde{v}_k^2, \quad (22)$$

and

$$T_n = \sum_k \tilde{\lambda}_k \left( \frac{1}{n_1} \sum_i \tilde{\psi}_k(x_i) - \frac{1}{n_2} \sum_j \tilde{\psi}_k(y_j) \right)^2. \quad (23)$$

The two averages over datasets  $X$  and  $Y$  are mutually independent, and both are asymptotically normal. This illustrates the limiting distribution of  $T_n$  which we prove in the next subsection.

### 3.3 Limiting distribution of $T_n$

We identify the limiting distribution of  $T_n$  is the following unified theorem, which implies particular limits under  $\mathcal{H}_0$  and  $\mathcal{H}_1$  in various setting of  $\|q - p\|$ . Consider the alternative  $q = p + \tau g$  for some fixed  $g = q_1 - p$ ,  $0 \leq \tau \leq 1$ , where  $q$  remains a probability density for any  $\tau$ . By the integrability of  $\tilde{\psi}_k$  under  $q_1(x)dx$  ((4) of Proposition 3.3), the constants

$$c_k = \int \tilde{\psi}_k(y)g(y)dy \quad (24)$$

are finite, and  $\sum_k \tilde{\lambda}_k c_k^2 < \infty$ . The bias  $\tilde{v}_k$  defined in Eqn. (21) can be written as  $\tilde{v}_k = -\tau c_k$ .

**Theorem 3.4.** *Notations as above,  $\tau = \tau_n$  may depend on  $n$  as  $n \rightarrow \infty$ . Under Assumption 1, as  $n = n_1 + n_2 \rightarrow \infty$  with  $\frac{n_1}{n} \rightarrow \rho_1 \in (0, 1)$ ,*

(1) *If  $\tau = O(n^{-1/2})$ , or  $\tau = o(n^{-1/2})$  including  $\tau = 0$ , then*

$$nT_n \xrightarrow{d} \sum_k \tilde{\lambda}_k (-ac_k + \xi_k)^2, \quad \xi_k \sim \mathcal{N}\left(0, \frac{1}{\rho_1} + \frac{1}{\rho_2}\right) \text{ i.i.d.},$$

where  $a = \lim_{n \rightarrow \infty} \tau_n \sqrt{n}$ , which is a constant when  $\tau \sim O(n^{-1/2})$  and otherwise zero. Due to the summability of  $\sum_k \tilde{\lambda}_k$  the random variable on the right hand side is well-defined.

(2) *If  $\tau = O(n^{-1/2+\delta})$ , where  $0 < \delta < \frac{1}{2}$ , then*

$$\frac{nT_n - n^{2\delta} \sum_k \tilde{\lambda}_k c_k^2}{n^\delta} \xrightarrow{d} \mathcal{N}(0, \sigma_{(2)}^2)$$

where  $\sigma_{(2)}^2 = 4 \sum_k \tilde{\lambda}_k^2 c_k^2 (\frac{1}{\rho_1} + \frac{1}{\rho_2})$ .

(3) *If  $\tau = 1$ ,  $g = q - p$ , then*

$$\sqrt{n}(T_n - \sum_k \tilde{\lambda}_k c_k^2) \xrightarrow{d} \mathcal{N}(0, \sigma_{(3)}^2)$$

where  $\sigma_{(3)}^2 = 4 \left( \frac{1}{\rho_1} \sum_k \tilde{\lambda}_k^2 c_k^2 + \frac{1}{\rho_2} \sum_{k,l} \tilde{\lambda}_k \tilde{\lambda}_l c_k c_l S_{kl} \right)$  with  $S_{kl} = \int \tilde{\psi}_k(y) \tilde{\psi}_l(y) q(y) dy - c_k c_l$ ,  $c_k$  defined in Eqn. (24), and  $\sigma_{(3)}^2 < \infty$ .

Considering the special cases where  $\tau = 0$  and  $\tau = 1$  we have the following

**Corollary 3.5.** Under  $\mathcal{H}_0$ , as  $n = n_1 + n_2 \rightarrow \infty$  with  $\frac{n_1}{n} \rightarrow \rho_1 \in (0, 1)$ ,

$$nT_n \xrightarrow{d} \sum_k \tilde{\lambda}_k \xi_k^2, \quad \xi_k \sim \mathcal{N}\left(0, \frac{1}{\rho_1} + \frac{1}{\rho_2}\right) \text{ i.i.d.}$$

When  $n_1 = n_2$ , the limiting density is  $4 \sum_k \tilde{\lambda}_k \chi_{1,k}^2$  where  $\chi_{1,k}^2$  are i.i.d.  $\chi_1^2$  random variables.

**Corollary 3.6.** Under  $\mathcal{H}_1$  with specific  $q \neq p$ ,  $g = q - p$ ,

$$\sqrt{n}(T_n - \mu_{(3)}) \xrightarrow{d} \mathcal{N}(0, \sigma_{(3)}^2)$$

where  $\mu_{(3)} = \sum_k \tilde{\lambda}_k \tilde{v}_k^2$ , and  $\sigma_{(3)}^2$  is defined as in (3) of Theorem 3.4. When  $n_1 = n_2$ ,  $\sigma_{(3)}^2 = 8 \text{Var}_{x,y}(\tilde{k}_1(x, y))$ , where  $\tilde{k}_1(x, y) = -\int (\tilde{k}(x, y') - \tilde{k}(y, y')) q(y') dy' = \sum_k \tilde{\lambda}_k \tilde{v}_k (\tilde{\psi}_k(x) - \tilde{\psi}_k(y))$ .

Corollary 3.5 is a direct result of (1) of Theorem 3.4, and Corollary 3.6 of (3) plus verifying the relationship  $\sigma_{(3)}^2 = 8 \text{Var}_{x,y}(\tilde{k}_1(x, y))$  by definition. The  $n_1 = n_2$  case of both corollaries are mentioned separately as they recover the classical result in V-statistics analysis (Theorem 6.4.1.B and Theorem 6.4.3 [22]). The technique of proving Theorem 3.4 very much follows that in Chapter 6 of [22] as well, where the key idea is to replace the two independent sets of summations  $\frac{1}{\sqrt{n_1}} \sum_i \tilde{\psi}_k(x_i)$  and  $\frac{1}{\sqrt{n_2}} \sum_j \tilde{\psi}_k(y_j)$  by Gaussian random variables via multi-variate CLT (Lemma A.1). The approach allows us to identify the convergence in distribution of  $T_n$  at different scales of  $n$  down to  $O(n^{-1})$  when  $\tau \sim O(n^{-1/2})$ , which is the critical regime.

*Proof of Theorem 3.4.* We introduce

$$\hat{h}_k = \frac{1}{\sqrt{n_1}} \sum_{i=1}^{n_1} \tilde{\psi}_k(x_i), \quad \hat{g}_k = \frac{1}{\sqrt{n_2}} \sum_{j=1}^{n_2} (\tilde{\psi}_k(y_j) + \tilde{v}_k),$$

where  $\mathbb{E}_{x \sim p} \tilde{\psi}_k(x) = 0$ ,  $\mathbb{E}_{y \sim q} (\tilde{\psi}_k(y) + \tilde{v}_k) = 0$ ,  $\mathbb{E}_{x \sim p} \tilde{\psi}_k(x) \tilde{\psi}_l(x) = \delta_{kl}$ , and  $\mathbb{E}_{y \sim q} (\tilde{\psi}_k(y) + \tilde{v}_k) (\tilde{\psi}_l(y) + \tilde{v}_l)$  defined to be  $S_{kl}^{(n)}$ . One can verify that (Appendix A) as  $n \rightarrow \infty$ ,  $S_{kl}^{(n)} \rightarrow \delta_{kl}$  for every  $(k, l)$  as long as  $\tau \rightarrow 0$ , which is the case in (1) and (2). In (3),  $S_{kl}^{(n)}$  does not change with  $n$  and equals  $S_{kl}$  as defined in the statement of the Theorem.

Using the above notations, we rewrite Eqn. (23) as

$$nT_n = \sum_k \tilde{\lambda}_k \left( -\tau_n \sqrt{n} c_k + \frac{1}{\sqrt{\rho_{1,n}}} \hat{h}_k - \frac{1}{\sqrt{\rho_{2,n}}} \hat{g}_k \right)^2, \quad (25)$$

where  $\rho_{1,n} = \frac{n_1}{n}$  and  $\rho_{2,n} = \frac{n_2}{n}$ . The random variables  $\{\hat{h}_k\}_k$  are independent from  $\{\hat{g}_k\}_k$ , and both are asymptotically normal for finite many  $k$ 's. The replacement lemma A.1 utilizes a truncation argument, based on the decaying of  $\tilde{\lambda}_k$ , to establish the convergence in distribution after replacing  $\hat{h}_k$  and  $\hat{g}_k$  by their normal counterparts, which we apply to the scenarios (1)-(3) respectively. Details left to Appendix A.  $\square$

As for the speed of convergence, Berry-Essen rate of the convergence to asymptotic normality has been proved for U-statistics in the non-degenerate case, and can be extended to the V-statistics as in the theorem below. This corresponding to the case where  $\tau = 1$  and  $n_1 = n_2$ . The following theorem was established in Sec 6 of [22], and we reproduce it in a simplified version for completeness.

**Theorem 3.7** (Theorem 6.4.3. [22] (modified)). *Under Assumption 1 and 2, when  $n_1 = n_2 = n$ , as  $n \rightarrow \infty$ ,*

$$\sup_{x \in \mathbb{R}} \left| \Pr \left[ \frac{\sqrt{n}(T_n - T)}{2\sqrt{C_1}} \leq x \right] - \Phi(x) \right| = O_k(n^{-1/2}), \quad (26)$$

where  $T$  is as in Eqn. (22),  $C_1 = \text{Var}_{x,y}(\tilde{k}_1(x,y)) > 0$ ,  $\tilde{k}_1(x,y)$  defined as in Corrolary 3.6,  $\Phi(x)$  stands for the c.d.f. of standard normal random variable, and the subscript  $k$  denotes that in the asymptotic bound the constant depends on  $k$ .

The proof is left to Appendix B. The above result may be extended to the case where  $n_1 \neq n_2$ . We postpone the investigation, along with the study of convergence speed when  $\tau$  scales with  $n$ , to the future. The comparison between the theoretical limiting distribution and empirical distribution of  $T_n$  when  $n$  equals a few hundreds is shown in Section 3.5.

### 3.4 Consistency and power of test

Under Assumption 2, the quantity  $\sum_k \tilde{\lambda}_k c_k^2 = \frac{T}{\tau^2}$  is strictly positive as  $c_k$  is not zero for some  $k$  by Proposition 3.1. Thus Theorem 3.4 implies the consistency of the two sample test based on  $T_n$  (against a specific departure) as long as  $\tau \sim n^{-1/2+\delta}$  and  $\delta > 0$ :

**Theorem 3.8.** *Notations as above, under Assumption 1 and 2, for specific  $g = q_1 - p$  fixed, if  $\tau_n = O(n^{-1/2+\delta})$  where  $0 < \delta \leq \frac{1}{2}$  ( $\delta = \frac{1}{2}$  means that  $\tau = 1$ ), the test power  $\pi_n(p + \tau_n g) \rightarrow 1$  as  $n \rightarrow \infty$ .*

*Proof.* By (1) of Theorem 3.4, under  $\mathcal{H}_0$ ,  $nT_n$  converges in distribution to a random variable which has finite mean and variance, which means that the threshold  $t_\alpha$  in Eqn. (17) can be set as  $\frac{t_{(0)}}{n}$  where  $t_{(0)}$  is an absolute constant. Here we assume case (2) or (3) of Theorem 3.4. In both cases, the mean of  $T_n$  is asymptotically  $\theta \cdot n^{-1+2\delta}$  with  $\theta = \sum_k \tilde{\lambda}_k^2 c_k^2 > 0$  (means that  $n^{1-2\delta} T_n \rightarrow \theta$ ), and the distribution of  $(T_n - \mathbb{E}T_n)$  lies in the scale of  $O(n^{-1+\delta})$ . Then for any  $\epsilon$ -left-quantile of  $T_n | \mathcal{H}_1$ , namely for any  $\epsilon > 0$ ,  $r_\epsilon$  s.t.  $\Pr[T_n < r_\epsilon | q = p + \tau_n g] = \epsilon$ ,  $r_\epsilon$  asymptotically equals

$$\theta n^{-1+2\delta} - t_{(1)} n^{-1+\delta} = n^{-1+\delta} (\theta n^\delta - t_{(1)}), \quad (27)$$

where  $t_{(1)}$  is an absolute constant. Eqn. (27) is asymptotically larger than  $n^{-1+\delta} M$  for any  $M > 0$ , due to that  $\theta > 0$  and  $\delta > 0$ , and thus larger than  $t_\alpha = \frac{t_{(0)}}{n}$ . This proves that the power  $\pi_n(p + \tau_n g) \rightarrow 1$ .  $\square$

The following theorem proves the convergence rate for  $\tau = 1$  and  $n_1 = n_2$ , which is built upon Theorem 3.7 and a Chebyshev bound to control  $T_n$  under  $\mathcal{H}_0$  (Proposition B3). The proof is left to Appendix B.

**Theorem 3.9.** *Notations as above, under Assumption 1 and 2, for specific  $q \neq p$  and  $n_1 = n_2$ ,  $\pi_n(q) \rightarrow 1$  as  $n \rightarrow \infty$  with a rate at least  $O_k(n^{-1/2})$ , where the subscript  $k$  means that the constant in front depends*

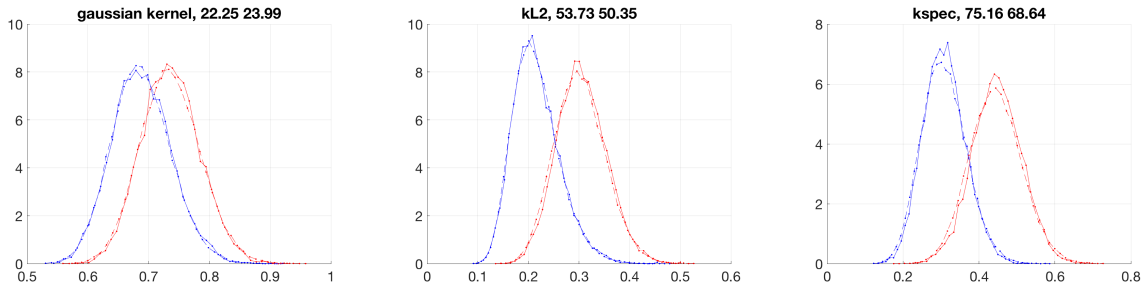


Figure 4: Empirical distribution of the statistic  $T_n$  under  $\mathcal{H}_0$  (blue) and  $\mathcal{H}_1$  (red) shown in comparison with the large  $n$  limiting distribution (broken lines) as in Theorem 3.4, for gaussian kernel (top right),  $k_{L^2}$  (bottom left) and  $k_{\text{spec}}$  (bottom right). The numbers are the fraction of  $T_n|\mathcal{H}_1$  lying to the right of the 0.95-quantile of  $T_n|\mathcal{H}_0$ , for empirical and theoretical curves respectively. Data sets  $X$  and  $Y$  drawn from  $p$  and  $q$  in the example in Section 3.5, a scatter plot is shown in Figure 6.

on the kernel  $k$ .

The consistency results like above for the new statistics is not surprising, and not very different from those of the KDE-based distance statistics [1]. The different power of the different kernels, which is the main concern of the paper, is better understood by investigating the factors which contribute to the power of the test statistic. As shown in the proof of the Theorem, the power is determined by the quantile of the distribution of  $T_n$  under  $\mathcal{H}_0$  and  $\mathcal{H}_1$  respectively. Particularly, quantities like  $E[T_n|\mathcal{H}_0]$ ,  $\text{Var}(T_n|\mathcal{H}_0)$ ,  $E[T_n|\mathcal{H}_1]$  and  $\text{Var}(T_n|\mathcal{H}_1)$  are very informative. As those quantities are determined by the eigenvalues  $\tilde{\lambda}_k$  and the per-eigen-mode “bias”  $\tilde{v}_k$ , we can compute these numbers so as to compare different kernels, which is next subsection.

### 3.5 Comparison of kernels

We consider the 2-dimensional example in the first section of the paper. Specifically,  $p$  is the uniform distribution on the curve  $\{(\cos \frac{\pi}{2}t, \sin \frac{\pi}{2}t), 0 \leq t \leq 1\}$  convolved with  $N(0, \epsilon_x^2 I_2)$ ,  $\epsilon_x = 0.02$ , and  $q$  is the distribution of the shifted curve  $\{((1 - \delta) \cos \frac{\pi}{2}t, (1 - \delta) \sin \frac{\pi}{2}t), 0 \leq t \leq 1\}$  convolved with  $N(0, \epsilon_x^2 I_2)$ , where  $\delta = 0.02$ . One realization of 200 points in  $X$  and  $Y$  is shown in Figure 6. <sup>1</sup> Let  $g = q - p$ , we consider the one-parameter family of alternative  $q = p + \tau g$ , and will simulate in the critical regime where the test power is less than 1. We assume that  $n_1 = n_2$  and denote by  $n$  in this subsection.

We will consider three kernels: (1) the gaussian kernel  $k_g(x, y) = e^{-\|x-y\|^2/2\epsilon_x^2}$ , (2) the one induced by the anisotropic kernel  $k_{L^2}(x, y) = \int a(r, x)a(r, y)dr$ , where  $dr$  is set to be the Lebesgue measure, and  $\Sigma_r$  is constructed so that the tangent direction is the first principle direction with variance  $0.2^2$ , and the normal direction is the second principle direction with variance  $\epsilon_x^2$ , and (3) the spectral filtered kernel as in Eqn. (11) where  $f_k$  are designed to be 1 for  $1 \leq k \leq 10$  and smoothly decays to zero at  $k = 20$ . For

<sup>1</sup>Strictly speaking  $p$  and  $q$  are longer compacted supported due to convolving with the 2-dimensional gaussian distribution, however, the normal density exponentially decays and  $\epsilon_x$  is small, so that there is not any practical difference. The analysis can extend by a truncation argument.

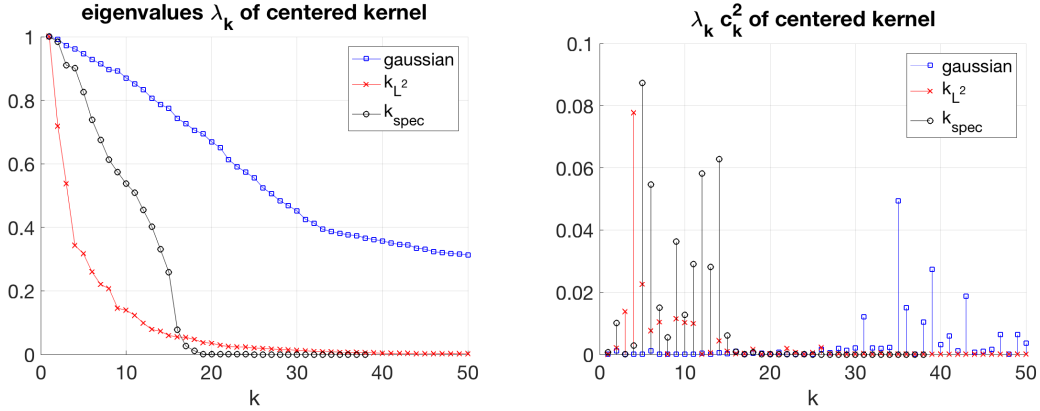


Figure 5: (Left) Eigenvalues  $\tilde{\lambda}_k$  of the three kernels: gaussian,  $k_{L^2}$  and  $k_{\text{spec}}$ . (Right) Product  $\tilde{\lambda}_k c_k^2$  where  $c_k$  is the bias for mode  $k$  as explained in Section 3.5.

each kernel, the quantities of interest are

$$\begin{aligned}\theta_0 &= E[T_n|\mathcal{H}_0], & \theta_1 &= E[T_n|\mathcal{H}_1], \\ \sigma_0^2 &= \text{Var}(T_n|\mathcal{H}_0), & \sigma_1^2 &= \text{Var}(T_n|\mathcal{H}_1).\end{aligned}$$

By Theorem 3.4, they can be approximated by the following, recalling that  $\tilde{v}_k = -\tau c_k$ ,

$$\bar{\theta}_0 = \frac{2}{n} \sum_k \tilde{\lambda}_k, \quad \bar{\theta}_1 = \sum_k \tilde{\lambda}_k \tilde{v}_k^2 + \frac{2}{n} \sum_k \tilde{\lambda}_k,$$

notice that the gap  $\bar{\theta}_1 - \bar{\theta}_0 = \sum_k \tilde{\lambda}_k \tilde{v}_k^2$ , which is the population  $T$ , is actually same as  $\theta_1 - \theta_0$ ; and

$$\bar{\sigma}_0^2 = \text{Var}\left(\sum_k \tilde{\lambda}_k \frac{1}{n} (h_k - g_k)^2\right), \quad \bar{\sigma}_1^2 = \text{Var}\left(\sum_k \tilde{\lambda}_k \left(\tilde{v}_k + \frac{1}{\sqrt{n}} (h_k - g_k)\right)^2\right)$$

where  $h_k, g_k \sim N(0, 1)$  i.i.d. and we use the result (i) in Theorem 3.4 to approximate  $\bar{\sigma}_1^2$ . All kernels are multiplied by a constant to make the largest eigenvalue  $\tilde{\lambda}_1 = 1$  so as to be comparable. The key quantity related the test power is the ratio

$$r = \frac{\theta_1 - \theta_0}{\sigma_1 + \sigma_0}.$$

In all experiments, the quantities  $\theta_0$ ,  $\theta_1$ ,  $\sigma_0$  and  $\sigma_1$  are computed by Monte-Carlo simulation over 10000 runs. Their asymptotic version (with bar) are computed by 50000 draws of the limiting distribution, truncating the summation over  $k$  to the first 500 terms; the values of  $\tilde{\lambda}_k$  and  $c_k = \int \tilde{\psi}_k(y)(q(y) - p(y))dy$  are approximated by the empirical eigenvalues and mean of eigenvectors over 10000 sample points drawn from  $p$  and  $q$  ( $\tilde{\psi}(y)$  is computed by Nystrom extension). The values of  $\tilde{\lambda}_k$  and  $c_k$  are shown in Figure 5, and those of  $\theta_0$  etc. in Table 1.

	$\theta_0$	$\theta_1$	$\sigma_0$	$\sigma_1$	$r$
$n = 200, \tau = 0.5$					
Gaussian	0.4771	0.5444	0.0677	0.0704	0.4874
	0.4754	0.5439	0.0676	0.0736	0.4848
$k_{L^2}$	0.0489	0.0958	0.0214	0.0306	0.9000
	0.0488	0.0939	0.0214	0.0312	0.8573
$k_{\text{spec}}$	0.0985	0.2046	0.0348	0.0587	1.1351
	0.0983	0.2013	0.0374	0.0620	1.0354
$n = 400, \tau = 0.5/\sqrt{2}$					
Gaussian	0.2381	0.2720	0.0334	0.0359	0.4885
	0.2379	0.2722	0.0339	0.0368	0.4850
$k_{L^2}$	0.0243	0.0477	0.0107	0.0153	0.8972
	0.0244	0.0471	0.0106	0.0157	0.8616
$k_{\text{spec}}$	0.0490	0.1036	0.0177	0.0305	1.1343
	0.0490	0.1003	0.0188	0.0310	1.0290

Table 1: The values of three kernels: gaussian,  $k_{L^2}$  and  $k_{\text{spec}}$ , in the example in Section 3.5. In first row are average over Monte-Carlo simulations, and in second row are the approximated values computed according to the limiting distribution identified by Theorem 3.4.

---

**Algorithm 1** Two-sample Test with Anisotropic-kernel MMD (AKMMD)

---

**Input:** Datasets  $X$  and  $Y$ , function handle  $a(r, x)$ ,  $n_{\text{boot}}$ , data points  $x_{\text{witness}}$

**Output:** Acceptance/Rejection of  $\mathcal{H}_0$ , the witness function evaluated on  $x_{\text{witness}}$

**External:** Subroutines AKMMD, AKWITNESS

- 1: **function** TWOSAMPLETEST( $X, Y, a, n_{\text{boot}}, x_{\text{witness}}$ )
  - 2:    $n_1 \leftarrow \text{size}(X), n_2 \leftarrow \text{size}(Y), n_R \leftarrow \text{size}(R)$
  - 3:   Compute matrix  $A_X \leftarrow \{a(r, x)\}_{r \in R, x \in X}$  and  $A_Y \leftarrow \{a(r, y)\}_{r \in R, y \in Y}$     $\triangleright a(r, x)$  as in (1)
  - 4:    $T, T_{\text{null}} \leftarrow \text{AKMMD}(A_X, A_Y, n_{\text{boot}})$     $\triangleright$  Subroutine to compute MMD with permutation
  - 5:    $\alpha \leftarrow 0.05, t_\alpha \leftarrow$  the  $(1 - \alpha)$ -quantile of  $T_{\text{null}}$     $\triangleright \alpha$  is the level of Type I error
  - 6:    $\text{Reject} \leftarrow (T > t_\alpha)$     $\triangleright \text{Reject}$  is a Boolean variable
  - 7:    $w \leftarrow \text{AKWITNESS}(A_X, A_Y, a, x_{\text{witness}})$     $\triangleright$  Subroutine to compute witness function
  - 8:   **return**  $\text{Reject}, w$
  - 9: **end function**
- 

## 4 Practical Considerations

Algorithm 1 gives the pseudo code for two-sample test based on the proposed MMD statistics, where two external subroutines, AKMMD and AKWITNESS, are to be specified. These functions for  $T_{L^2}$  (and  $T_{\text{spec}}$ ) are given in Algorithm 2 (Algorithm 3), where to call MMD-SPEC and WITNESS-SPEC, it needs to provide another input parameter  $f$  which is a positive vector of length  $r_f$  ( $r_f < \min\{n_1 + n_2, n_R\}$ ).  $f$  is the target spectrum of the kernel  $k_{\text{spec}}$  in Eqn. (11). Both algorithms compute the threshold  $t_\alpha$  by bootstrapping, and assume that the reference set  $R$  with  $\{\Sigma_r\}_{r \in R}$  is predefined.

In the rest of the section, we explain the bootstrapping approach, the empirical estimator of the witness function, and the construction of reference set in detail. We close the section by commenting on the computation complexity.

---

**Algorithm 2** Methods for  $k_{L^2}$ -MMD

---

```
1: function MMD-L2(  $A_X, A_Y, n_{\text{boot}}$  )
2:   Concatenate  $A \leftarrow [A_X \mid A_Y]$  ▷  $A$  is  $n_R$ -by- $(n_1 + n_2)$ 
3:   For  $i = 1, \dots, n_R$ ,  $h_X[i] \leftarrow \frac{1}{n_1} \sum_{j=1}^{n_1} A[i, j]$ ,  $h_Y[i] \leftarrow \frac{1}{n_2} \sum_{j=n_1+1}^{n_1+n_2} A[i, j]$ ,
4:    $T \leftarrow \frac{1}{n_R} \sum_{i=1}^{n_R} (h_X[i] - h_Y[i])^2$  ▷ Empirical MMD
5:   for  $k = 1$  to  $n_{\text{boot}}$  do
6:      $A_{\text{permute}} \leftarrow A$  with random permuted columns
7:     For  $i = 1, \dots, n_R$ ,  $h_X[i] \leftarrow \frac{1}{n_1} \sum_{j=1}^{n_1} A_{\text{permute}}[i, j]$ ,  $h_Y[i] \leftarrow \frac{1}{n_2} \sum_{j=n_1+1}^{n_1+n_2} A_{\text{permute}}[i, j]$ ,
8:      $T_{\text{null}}[k] \leftarrow \frac{1}{n_R} \sum_{i=1}^{n_R} (h_X[i] - h_Y[i])^2$  ▷ One sample of MMD under null hypothesis
9:   end for
10:  return  $T, T_{\text{null}}$ 
11: end function

12: function WITNESS-L2( $A_X, A_Y, a, Z$ )
13:  For  $i = 1, \dots, n_R$ ,  $h_X[i] \leftarrow \frac{1}{n_1} \sum_{j=1}^{n_1} A_X[i, j]$ ,  $h_Y[i] \leftarrow \frac{1}{n_2} \sum_{j=1}^{n_2} A_Y[i, j]$ ,
14:  Compute matrix  $A_Z \leftarrow \{a(r, x)\}_{r \in R, x \in Z}$ 
15:   $n_Z \leftarrow \text{size}(Z)$ , for  $j = 1, \dots, n_Z$ ,  $w[j] \leftarrow \frac{1}{n_R} \sum_{i=1}^{n_R} A_Z[i, j] (h_X[i] - h_Y[i])$ 
16:  return  $w$ 
17: end function
```

---

#### 4.1 Permutation test and choice of the threshold $t_\alpha$

The MMD statistics  $T$  introduced in Section 3 is non-parametric, which means that the threshold  $t_\alpha$  does not have a closed-form expression for finite  $n$ . In practice, one may use a classical method known as the *permutation test* [15], which is a bootstrapping strategy to empirically estimate  $t_\alpha$ , and previously used in RKHS MMD [12]. The idea is to model the null hypothesis by pooling the two datasets, resampling from that pool, and computing one instance of the MMD under that null hypothesis. Repetitive resampling thus corresponds to permuting the joint dataset multiple times, and it generates a sequence values of  $T$ , the  $(1 - \alpha)$ -quantile of which is used as  $t_\alpha$  (see both Algorithm 2 and Algorithm 3). Strictly speaking, the power of the test is slightly degraded due to the empirical estimate of the null hypothesis. However, as we see in Section 5, the test still yields very strong results in a number of examples.

Meanwhile, the limiting distribution of the statistics  $T_n$  appears to well approximate the empirical one under  $\mathcal{H}_0$ , as shown in Section 3.5. This suggests the possibility of determining  $t_\alpha$  based on the empirical spectral decomposition of the kernel. In the current work we focus on the bootstrapping approach (permutation test) for simplicity.

#### 4.2 Empirical witness functions

The population witness functions have been introduced in Section 2.3, and, by definition, can be evaluated at any data point  $x \in \Omega$ . For the kernel  $k_{L^2}$ , the empirical version of Eqn. (13) is

$$\hat{w}_{L^2}(x) = \frac{1}{n_R} \sum_{r \in R} a(r, x) (\hat{h}_X(r) - \hat{h}_Y(r)), \quad (28)$$

---

**Algorithm 3** Methods for  $k_{\text{spec}}$ -MMD

---

```
1: function MMD-SPEC( $A_X, A_Y, n_{\text{boot}}, f$ ) ▷  $f \in \mathbb{R}_+^{r_f}$  is the target eigenvalues
2:   Concatenate  $A \leftarrow [A_X \mid A_Y]$  ▷  $A$  is  $n_R$ -by- $(n_1 + n_2)$ 
3:    $U, S, V \leftarrow \text{SVD}(A, r_f)$  ▷  $USV^T$  is the best rank- $r_f$  approximation of  $A$ 
4:    $v_X \leftarrow \frac{1}{n_1}(V_{1:n_1,:})^T \mathbf{1}_{n_1}, v_Y \leftarrow \frac{1}{n_2}(V_{n_1+1:n_1+n_2,:})^T \mathbf{1}_{n_2}$  ▷  $\mathbf{1}_m$  is all-ones vector of length  $m$ 
5:    $T \leftarrow (v_X - v_Y)^T \text{Diag}\{f\}(v_X - v_Y)$  ▷ Empirical MMD
6:   for  $k = 1$  to  $n_{\text{boot}}$  do
7:      $V_{\text{permute}} \leftarrow V$  with random permuted rows
8:      $v_X \leftarrow \frac{1}{n_1}(V_{1:n_1,:})^T \mathbf{1}_{n_1}, v_Y \leftarrow \frac{1}{n_2}(V_{n_1+1:n_1+n_2,:})^T \mathbf{1}_{n_2}$ 
9:      $T_{\text{null}}[k] \leftarrow (v_X - v_Y)^T \text{Diag}\{f\}(v_X - v_Y)$  ▷ One sample of MMD under null hypothesis
10:  end for
11:  return  $T, T_{\text{null}}$ 
12: end function

13: function WITNESS-SPEC( $A_X, A_Y, a, Z, f$ )
14:   Concatenate  $A \leftarrow [A_X \mid A_Y], U, S, V \leftarrow \text{SVD}(A, r_f)$ 
15:    $v_X \leftarrow \frac{1}{n_1}(V_{1:n_1,:})^T \mathbf{1}_{n_1}, v_Y \leftarrow \frac{1}{n_2}(V_{n_1+1:n_1+n_2,:})^T \mathbf{1}_{n_2}$ 
16:   Compute matrix  $A_Z \leftarrow \{a(r, x)\}_{r \in R, x \in Z}$ 
17:    $V_Z \leftarrow S^{-1}U^T A_Z$  ▷  $V_Z$  is  $r_f$ -by- $n_Z, n_Z$  the size of  $Z$ 
18:    $w \leftarrow V_Z^T \text{Diag}\{f\}(v_X - v_Y)$ 
19:   return  $w$ 
20: end function
```

---

which can be computed straightforwardly from the empirical histograms  $\hat{h}_X, \hat{h}_Y$  and the pre-defined kernel  $a(r, x)$ , see Algorithm 2.

For the kernel  $k_{\text{spec}}$ , Eqn. (14) is approximated by

$$\hat{w}_{\text{spec}}(x) = \sum_k f_k \hat{\psi}_k(x) \left( \frac{1}{n_1} \sum_{i=1}^{n_1} \hat{\psi}_k(x_i) - \frac{1}{n_2} \sum_{j=1}^{n_2} \hat{\psi}_k(y_j) \right), \quad (29)$$

where  $\hat{\psi}_k(x_i), \hat{\psi}_k(x_j)$  are computed by SVD of the asymmetric kernel matrix, and the out-of-sample extension to  $\hat{\psi}_k(x)$  by Nystrom method, see Algorithm 3.

### 4.3 Sampling of the reference set

In bio-informatics applications e.g. flow cytometry, datasets are usually large in volume so that one can construct the reference set  $R$  and covariance field  $\{\Sigma_r\}_r$  from a pool of data points, which combines multiple samples, before the differential analysis in which MMD is involved. In some application scenario (like diffusion MRI),  $R$  and  $\{\Sigma_r\}_r$  are provided by external settings. Thus we treat the procedure of constructing  $R$  and  $\{\Sigma_r\}_r$  separately from the two-sample analysis, which is also assumed in the theory.

In experiments in this work, we sample the reference points randomly in Lebesgue measure using the following heuristic: given a pool of data points e.g. drawn from  $p$  and  $q$  or subsampled from larger

datasets, the procedure loops over batches until  $n_R$  points have been generated. In each loop, a batch of points are loaded from the pool, and candidate points are sampled from the batch according to  $p_i^{-1}$  which is the KDE of each point in the batch. The candidate points are giggled, and points which have too few neighbors in the pool dataset are excluded. The code can be found in the software XXX.

The covariance fielded is computed by local PCA, when needed. This is related to the issue of “ $\sigma$ -selection” in gaussian MMD [12], where a “median heuristic” was proposed to determine the  $\sigma$  in the gaussian kernel  $k_\sigma(x) = e^{-\|x\|^2/2\sigma^2}$ . In our setting, the extension of “ $\sigma$ ” is the local covariance matrix  $\Sigma_r$ , which allows different  $\sigma$  at different points, apart from different  $\sigma$  along different local directions. In estimating  $\Sigma_r$ , a controlling parameter is then the size of the local neighborhood, i.e. the  $k$ -nearest neighbors from which local PCA is computed. In the manifold setting, there are strategies to choose  $k$  so as to most efficiently estimate local covariance matrix, see e.g. [18], and it is best done by using different  $k$  at different point. For simplicity, in all the experiments we set  $k$  to be a fraction of the total number of samples, which may be sub-optimal. We also introduce a parameter  $\tilde{\sigma} > 0$  and set  $\Sigma_r = \tilde{\sigma}^2 \Sigma_r^0$ , where  $\Sigma_r^0$  is computed via local PCA, so as to make the “size” of  $\Sigma_r$  tunable. The parameter  $\tilde{\sigma}$  is sampled on a binary grid ( $2^k$  for  $k = -2, \dots, 2$ ).

#### 4.4 Computational complexity

We will only discuss the cost of computing the MMD statistics, namely that of MMD-L2 (Algorithm 2) and MMD-SPEC (Algorithm 3). The extra cost for computing the witness function is negligible, as can be seen from the code (some computation, e.g. that of  $h_X$  and  $h_Y$  in WITNESS-L2, and the SVD of  $A$  in WITNESS-SPEC are repetitive for illustrative purpose.)

We firstly discuss MMD-L2: The cost for computing one empirical MMD statistics  $T$  is of  $O(n \cdot n_R)$ , where  $n = n_1 + n_2$  is the size of the two samples. The main cost is the one-time construction of the asymmetric kernel matrix  $A = [A_X | A_Y]$ , which also dominates the memory requirements. While the choice of the reference set, and hence the number of reference points  $n_R$ , is related to the problem being addressed, any amount of structure in the samples leads to a choice of  $n_R$  that is  $o(n)$ . This yields major computational and memory benefits as the test complexity is much smaller than the  $O(n^2)$ , which is the order for computing the U-statistics via a symmetric gaussian kernel without extra techniques. In all applications we’ve considered and synthetic examples we’ve worked with,  $n_R$  is in the tens or hundreds, and can remain relatively constant as  $n$  grows while still yielding a test with large power. This means the test with an anisotropic kernel becomes linear in the number of points being tested.

In MMD-SPEC, the extra computation is for the rank- $r_f$  SVD of matrix  $A$ . While the traditional full SVD costs  $O(n_R n^2)$ , the rank- $k$  SVD can be computed in time  $O(nn_R \log k + nk^2)$  by modern randomized algorithms (see e.g. [25]) assuming the  $(k + 1)$ -th singular value is small, which is the case where the proposed approach is most useful.

The computational cost may be furtherly reduced by exploring the sparse/low-rank structure of the kernel matrix  $A$ . When  $\{\Sigma_r\}_r$  are mostly supported on a local neighborhood, each row of  $A$  only has a small

number of non-zeros. Suppose that the rows of  $A$  are  $k$ -sparse, the computation of  $A$  can be accelerated by employing fast nearest neighbor search (by Kd-tree or randomized algorithm) in the local Mahalanobis distance, which reduces the storage to  $O(n_R k)$ . Meanwhile, when  $A$  has a small numerical rank, e.g. only  $k$  singular values are significantly zero,  $A$  can be stored in its rank- $k$  factorized form  $(U, S, V)$  which is computed in linear time of  $n$ , as analyzed above for MMD-SPEC. This will save computation in bootstrapping as both  $T_{L^2}$  and  $T_{\text{spec}}$  can be computed from  $S$  and (row-permuted)  $V$  only.

## 5 Applications

### 5.1 Synthetic examples

#### 5.1.1 Example 1: Curve in 2 dimension

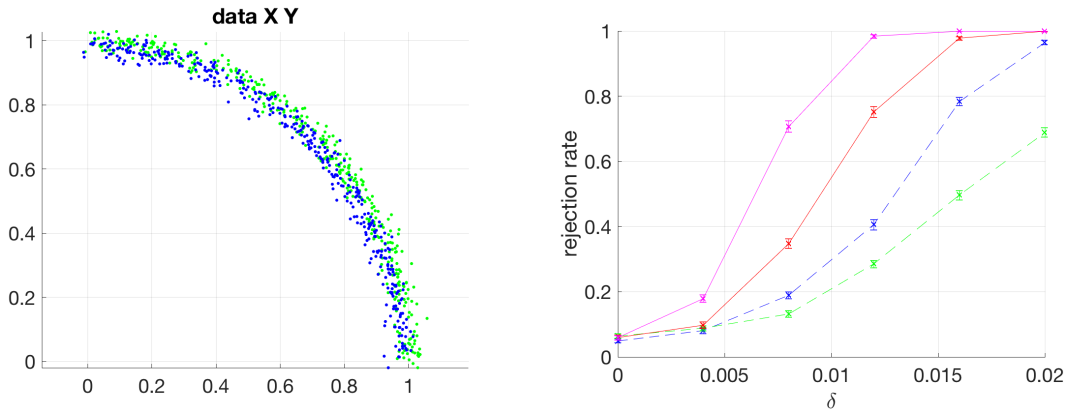


Figure 6: Example 1 in Section 5.1, two curves in  $\mathbb{R}^2$ . (Left) Two samples  $X$  and  $Y$  in  $\mathbb{R}^2$  in green and blue respectively. (Right) testing power of (blue) MMD using gaussian kernel, (green) summed KS distance from 20 random projections to 1D, (red) MMD using anisotropic kernel  $k_{L^2}$ , (pink) MMD using spectral-filtered anisotropic-kernel  $k_{\text{spec}}$ .

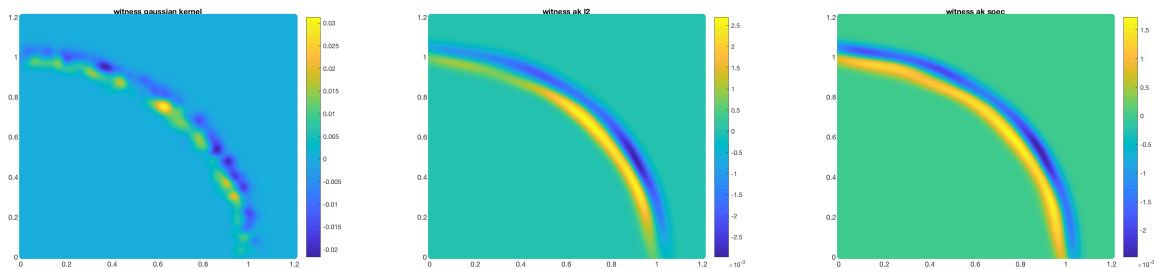


Figure 7: Witness functions of (left) gaussian kernel, (middle)  $k_{L^2}$  and (right)  $k_{\text{spec}}$  respectively, in the two sample test in Figure 6.

The density  $p$  is the uniform distribution on a quarter circle with radius 1 convolved with  $\mathcal{N}(0, \epsilon_x^2)$ ,  $q$  on a quarter circle with radius  $1 - \delta$  convolved with  $\mathcal{N}(0, \epsilon_x^2)$ , which is the same example in Section 3.5 (top left in Figure 4),  $\epsilon_x = 0.02$ . The departure is parametrized by  $\delta > 0$ , taking values from 0 to 0.02. The rejection rate is computed from the average over 1000 runs according to Algorithm 1, as shown in the left of Figure 6, where the errorbars indicate the standard deviation. For the gaussian kernel, the curve corresponds to the  $\sigma$  which has the best performance over a grid, and it is obtained by an intermediate value on the grid. The witness functions of the three kernels when  $\delta = 0.2$  are computed according to Section 4.2, and shown in Figure 7.

### 5.1.2 Example 2: Gaussian mixture in 3 dimension

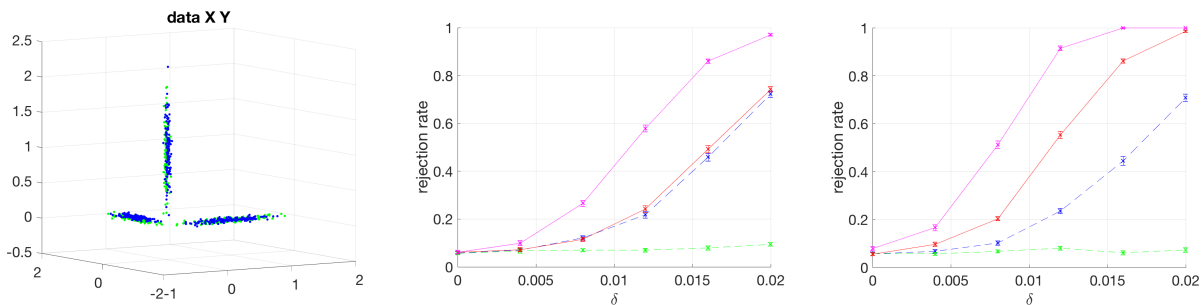


Figure 8: Example 2 in Section 5.1: two gaussian mixtures in  $\mathbb{R}^3$ . (Left) two samples, (Middle) testing power using  $\{\Sigma_r\}_r$  determined by local covariance estimation, (Right) testing power using  $\{\Sigma_r\}_r$  by the true covariance matrix of the belonging cluster.

Two gaussian mixtures in  $\mathbb{R}^3$ ,  $n_1 = n_2 = 200$ ,  $n_R = 100$ . The density  $p$  consists of 3 equal-size components centering at  $(1, 0, 0)^T$ ,  $(0, 1, 0)^T$  and  $(0, 0, 1)^T$  respectively, with diagonal covariance matrix  $\text{diag}\{(\frac{1}{3})^2, \epsilon_x^2, \epsilon_x^2\}$ ,  $\text{diag}\{\epsilon_x^2, (\frac{1}{3})^2, \epsilon_x^2\}$  and  $\text{diag}\{\epsilon_x^2, \epsilon_x^2, (\frac{1}{3})^2\}$ ,  $\epsilon_x = 0.02$ ; and density  $q$  differs from  $p$  by centering the three means at  $(1, \delta, 0)^T$ ,  $(0, 1, \delta)^T$  and  $(\delta, 0, 1)^T$ , while letting the covariance matrices remain the same. The constant  $\delta$  takes value from 0 to 0.02. Results shown in Figure 8, similar to Figure 6.

## 5.2 Flow cytometry data analysis

Flow Cytometry is a laser based technology used for cell counting. It is routinely used in diagnosing blood diseases by measuring various physical and chemical characteristics of the cells in a sample. This leads to each sample being represented by a multi-dimensional point cloud of tens of thousands of cells that were measured.

Two natural questions arise in comparing various flow cytometry samples. The first is a supervised learning question: can a statistical test detect the systemic differences between a set of healthy people and a set of unhealthy people? The second question is an unsupervised learning question: can the distance measure

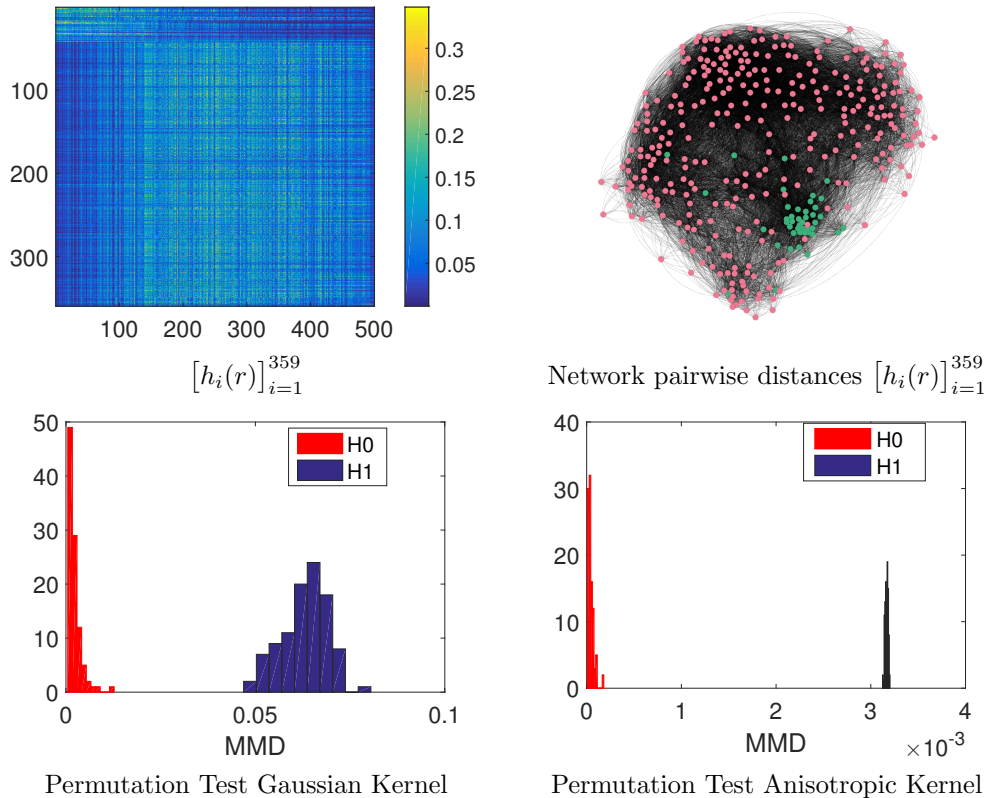


Figure 9: Top: Unsupervised histograms and clustering of AML patients. Bottom: Two sample test between pool of healthy and unhealthy patients comparing isotropic and anisotropic gaussian.

be used to determine the pairwise distance between any two samples, and will that distance matrix yield meaningful clusters?

We address both of these questions for data from the public competition Flow Cytometry: Critical Assessment of Population Identification Methods II (FlowCAP-II). This dataset consists of 316 healthy patients and 43 patients with Acute myeloid leukemia (AML), where each person has approximately 30,000 cells measured across 7 physical and chemical features. We compare isotropic gaussian MMD to anisotropic MMD and demonstrate, in all cases, our anisotropic MMD test has more power and yields more accurate unsupervised clusters. We only show the pairwise distance embedding for the reference set asymmetric kernel  $a(r, x)$  due to the untenable  $O(n^2)$  cost of computing each of the  $\binom{k}{2}$  pairs.

Acute myeloid leukemia (AML) is a cancer of the blood that is characterized by a rapid growth of abnormal white blood cells. While being a relatively rare disease, it is incredibly deadly with a five-year survival rate of 27% [8]. AML is diagnosed through a flow cytometry analysis of the bone marrow cells, and while there are features that distinguish AML in certain cases, other cases can be more difficult to detect. State of art supervised methods include SPADE, Citrus, etc. See [5] and the references therein.

We use an anisotropic kernel with only 500 reference points. We create an unsupervised clustering by

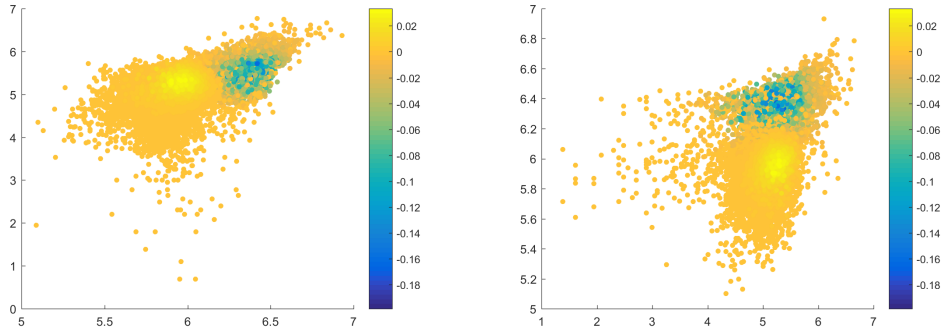


Figure 10: Two two-dimensional slices of the 7 dimensional point cloud, colored by the witness function between healthy patients and those with AML. Positive values are more indicative of AML.

computing the pairwise distances  $d^2[i, j] = T_{L^2}$  between person  $i$  and person  $j$ . In Figure 9, we display the network of these people constructed by weighting each edge as the exponential of the negative distance  $d^2[i, j]$  properly scaled. When supervising the process and running a two sample test between the pool of healthy cells and the pool of unhealthy cells, we see that the anisotropic kernel yields significantly better separation and lower variance than the isotropic gaussian kernel.

We also examine the witness function in Figure 10 that is generated by the anisotropic kernel, as introduced in Section 2.3. This yields a tool for visualizing the separation between the two samples in the original data space. This gives a way to communicate the decision boundary to the medical community, which uses visualization of the 2D slices as the diagnostic tool for determining whether the patient as AML.

### 5.3 Diffusion MRI imaging analysis

Diffusion weighted MRI is an imaging modality that creates contrast images via the diffusion of water molecules. Various regions of the brain diffuse in different ways, and the patterns can reveal details about the tissue architecture. At a low level, each pixel in a 3D brain image generates a 3D diffusion tensor (i.e. covariance matrix) that describes the local flow of water molecules.

An important question in diffusion MRI analysis is to identify regions of the brain that systemically differ between groups of healthy and sick individuals. We attack this problem by comparing the distributions of the diffusion tensors in various regions of the brain, thus framing it as a multiple sample problem. Every brain is co-registered so that the pixels overlap.

Real images are around  $200 \times 200 \times 200$ , so the amount of memory needed to build a square symmetric kernel, even a sparse one, is completely prohibitive. For this reason, we instead consider a set of reference pixels  $R$  that subsamples the image, and construct an anisotropic kernel  $a : (X, T) \rightarrow R \rightarrow [0, 1]$ , where  $x_i$  is the location of pixel  $i$  and  $T_{x_i}$  is the  $3 \times 3$  diffusion tensor at pixel  $i$ . This kernel must enforce both locality in the pixel space, and the local behavior of the diffusion tensors. The latter requires measuring

covariance matrices over the space of positive semi-definite matrices.

Fortunately, the study of covariance matrices on the space of positive semi-definite matrices is a well studied phenomenon [2]. The main takeaway is that there is an isomorphism from a  $3 \times 3$  diffusion tensor  $T$  and its vectorized representation

$$\gamma = \begin{bmatrix} T_{11} & T_{22} & T_{33} & \sqrt{2}T_{12} & \sqrt{2}T_{13} & \sqrt{2}T_{23} \end{bmatrix}.$$

Thus, we can define a  $6 \times 6$  covariance matrix  $\Sigma_{T_i}$  on  $\gamma$  and define the anisotropic kernel

$$a_{i,r} = \exp\{-(\gamma_i - \gamma_r)\Sigma_r^\dagger(\gamma_i - \gamma_r)^\top\} \cdot \mathbb{1}_{\|x_i - r_i\| < \epsilon}. \quad (30)$$

We examine MMD using a synthetic data set generated from the common brain phantom image. We treat this as a 2D slice of the 3D image, and simply have all tensor variation in the z-direction constant and uncorrelated with the xy-direction of this slice. We also assume that the brains have been co-registered. The process of co-registration is an independent preprocessing issue which can be incorporated into our proposed methodology when working with real world data sets, but is outside the scope of this paper.

In Figure 11, we show both a “healthy” brain and an “unhealthy” brain in which a small region has been removed. The intensity of the image in this case will correspond to the eccentricity of the diffusion tensor at that point; the magnitude of the tensor will decrease from left to right in the same way for both images and the angle shift uniformly from left to right. The eccentricity, magnitude, and angle all have iid Gaussian noise added to them with  $\sigma = 0.05$ .

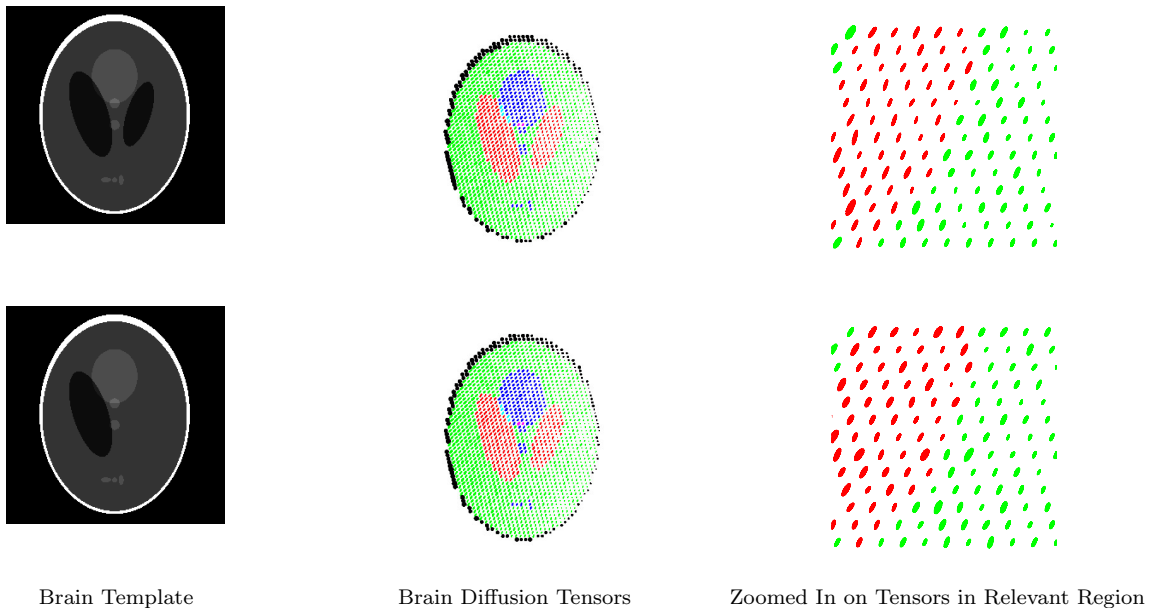


Figure 11: Examples of synthetic healthy and unhealthy brains. The coloring of the diffusion tensors is done for visual convenience. Top: “healthy class”, Bottom: “unhealthy class”.

We down-sample the brain by a factor of 5 for the reference points, and consider the mean embeddings  $h_i(r)$  for 10 realizations of a healthy brain (null hypothesis  $H_0$ ), and for 5 realizations of a healthy brain and 5 realizations of an unhealthy brain (alternative hypothesis  $H_1$ ). Figure 12 shows the supervised witness function of regions of difference between the two groups, as well as a permutation test in which we permute group labels while maintaining the individual brain structure. We also show the leading eigenvectors of the pairwise network generated by measuring the MMD between any two brains.

By using reference points, each brain is represented by a kernel that is  $65536 \times 2601$ , and the data adaptive MMD computation can be run on 10 brains in about 4.5 minutes on a standard laptop.

We also compare the anisotropic kernel to one with an isotropic kernel of constant bandwidth. We cannot compare to kernel MMD with a square symmetric kernel due to computational limits, so instead we compare to the modified asymmetric kernel as in (30), but without the covariance matrix. Instead, we replace by a constant bandwidth, which is chosen to be  $\sigma^2 = \mathbb{E}_{r \in R}[\text{trace}(\Sigma_r)]$ .

## 6 Discussion and Remarks

As a summary, the paper studies kernel-based MMD statistics where the kernel  $k(x, y)$  is of the form of  $\int a(r, x)a(r, y)d\mu_R(r)$ , and generally involving another filtering kernel over  $r$ . The statistics can be computed with a pre-defined reference set in time  $O(n_R n)$ , where  $n$  is the number of samples and  $n_R$  is the cardinal number of the reference set. The power of the test against alternative distributions is analyzed using the spectral decomposition of the kernel with respect to the data distribution, and the asymptotic consistency is proved under generic assumptions. The difference in the testing power of the kernels are determined by their spectral properties. We apply the proposed methodology to flow cytometry and diffusion MRI data analysis, where the goal of analysis is formulated as comparing the distribution of multiple samples.

We close the section by a few remarks about the proposed approach as well as possible extensions:

**The spectral coordinates.** Both the spectral filtered kernel  $k_{\text{spec}}$  and the asymptotic analysis in Section 3 are closely related to the view of the kernel-MMD as certain  $L^2$  distance, weighted or unweighted, in the space of spectral embedding. Theoretically the latter is infinitely dimensional, however, in practice only finite dimensional coordinates may contribute to the RKHS MMD statistic - in the sense of providing sufficient information which exceeds the “noise level” due to finite-sample effect. Thus, the leading  $K$  coordinates of spectral embedding (depends on the kernel) gives a mapping from  $\mathbb{R}^d$  to  $\mathbb{R}^K$ , where  $K$  may be proportional or larger than  $d$ , and one may consider the two-sample test in the new coordinates. Under assumption of this paper, the general alternative will become a mean-shift alternative in the new coordinates. The spectral-filtered kernel uses a re-weighted  $L^2$  norm for this test, while there are other possibilities. The fact that the correlation between the coordinates are zero - under null hypothesis, and nearly zero with small deviated  $q$  - is favorable for this mean-shift detection problem.

**Weighting of bins.** We introduced the general-form statistics  $T_{\text{general}}$  (7), then focus on the particular

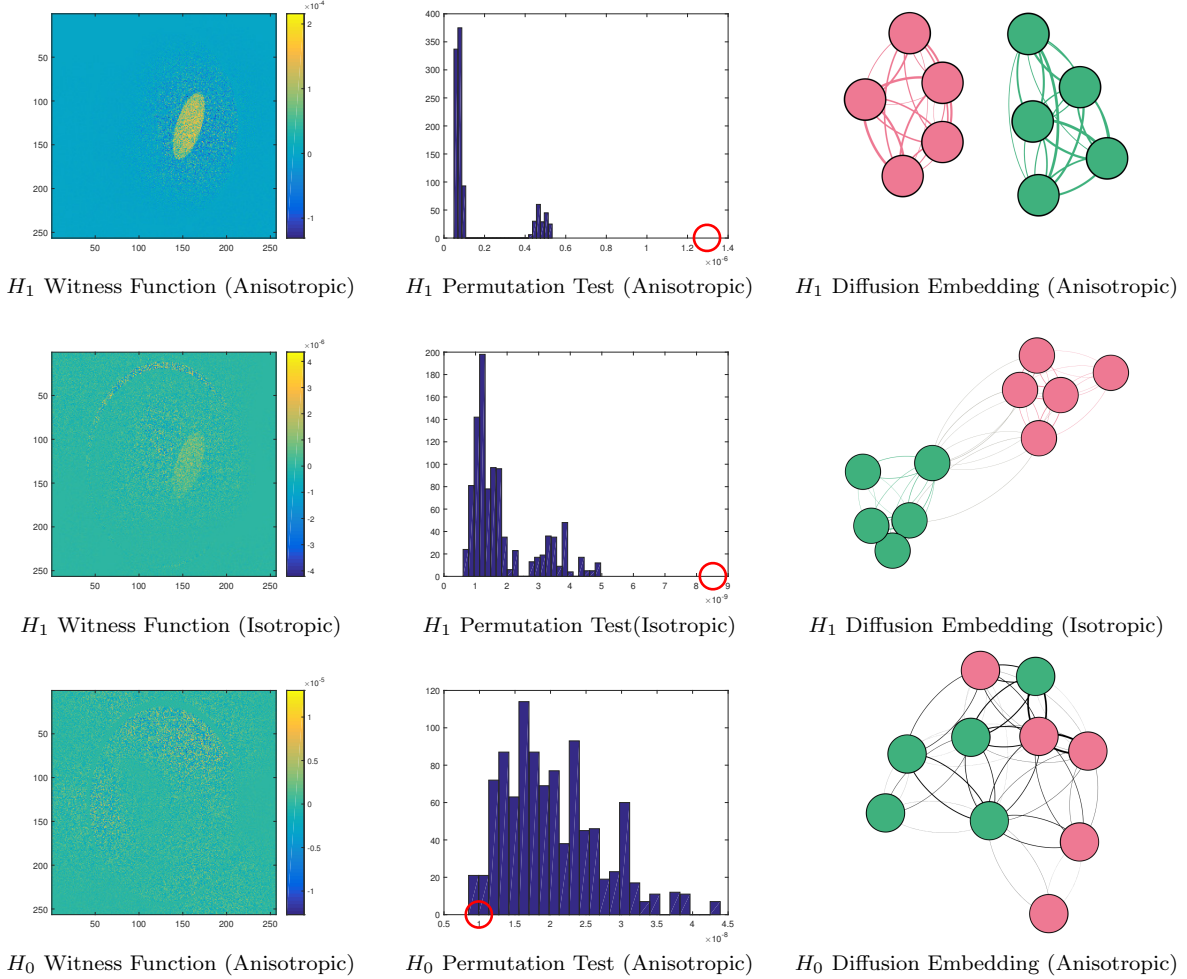


Figure 12: Witness function, permutation test for MMD, and pairwise diffusion embedding for alternative hypothesis with anisotropic kernels (top), alternative hypothesis with isotropic kernels (medium), and null hypothesis with anisotropic kernels (bottom) for two groups of 5 brains.

form of spectral-filtered kernel. While spectral filtering introduces weighting in the generalized Fourier domain, another important variation is to introduce weighting in the “real domain”, namely weighting each bin centered at  $r$  by a weight  $w(r)$ . Such weights may be computed from data, e.g. by certain local  $p$ -value (see below), where the dependence among  $r$ ’s needs to be handled. Another interesting question is how to introduce multi-resolution systems in the context of the current paper: On one hand, mapping points into spectral coordinates (which is integrating density  $p$  to spectral basis  $\int \psi_k(x)p(x)dx$ ) has certain advantage as analyzed above, however, spectral basis is global and may not be sensitive enough to local departure. On the other hand, histograms on local bins (which is integrating density  $p$  to local basis  $\int b_r(x)p(x)dx$  where  $b_r(x)$  is the “binning function” at point  $r$ ) may have large variance and one needs to jointly analyze multiple bins. By considering multi-scale basis on the graph formed by the reference set

may be a framework to overcome the shortcomings of both sides.

**Beyond  $L^2$  distance.** RKHS MMD considers the  $L^2$  distance by construction, while other metrics have been studied in literature, particularly the Wasserstein metric which has the interpretation of optimal flow given the underlying geometry. Such “geometric” distances are certainly useful in various application scenarios. Using the reference set, a modification of  $T_{L^2}$  will be

$$T_{\text{EMD}}(p, q) = \min_{\pi} \int \pi(r, r') d_R(r, r') d\mu_R(r) d\mu_R(r'),$$

$$\text{s.t.} \quad \int \pi(r, r') d\mu_R(r') = h_p(r), \quad \int \pi(r, r') d\mu_R(r) = h_q(r'),$$

where  $h_p, h_q$  are the population histograms, and  $d_R(r, r')$  is certain metric on reference set. It may also be possible to construct a metric which is equivalent to the Wasserstein metric by measuring the difference at reference points across multiple scales of covariance matrices, as is done with Haar wavelet [23] and with diffusion kernels [17]. Efficient estimation scheme of the Wasserstein metric needs to be developed as well as the consistency analysis with  $n$  samples.

**Local  $p$ -value.** The current approach gives a global test and computes the  $p$ -value for the hypothesis of the distribution globally. In certain applications, especially differential analysis of flow cytometry data and other single-cell data, a more-important problem is to find the local region where the two samples differ corresponding to different biological conditions, or in other words, to derive a “local”  $p$ -value of the test. While the witness function introduced in our current approach can provide indication where  $q \neq p$ , a more systematically study of testing the hypothesis locally and controlling false discovery rate across bins is needed.

## Acknowledgment

We would like to thank Yuval Kluger for introducing the problem of flow cytometry data analysis. We would also like to thank Carlo Pierpaoli, Neda Sadeghi, and Okan Irfanoglu for introducing the problem of diffusion MRI data analysis. Cloninger was supported by NSF grant DMS-1402254.

## References

- [1] Niall H Anderson, Peter Hall, and D Michael Titterton. Two-sample test statistics for measuring discrepancies between two multivariate probability density functions using kernel-based density estimates. *Journal of Multivariate Analysis*, 50(1):41–54, 1994.
- [2] Peter J Basser and Sinisa Pajevic. Spectral decomposition of a 4th-order covariance tensor: Applications to diffusion tensor mri. *Signal Processing*, 87(2):220–236, 2007.

- [3] Amit Bermanis, Amir Averbuch, and Ronald R Coifman. Multiscale data sampling and function extension. *Applied and Computational Harmonic Analysis*, 34(1):15–29, 2013.
- [4] Peter J Bickel. A distribution free version of the smirnov two sample test in the p-variate case. *The Annals of Mathematical Statistics*, 40(1):1–23, 1969.
- [5] Robert V Bruggner, Bernd Bodenmiller, David L Dill, Robert J Tibshirani, and Garry P Nolan. Automated identification of stratifying signatures in cellular subpopulations. *Proceedings of the National Academy of Sciences*, 111(26):E2770–E2777, 2014.
- [6] Herman Callaert and Paul Janssen. The berry-esseen theorem for u-statistics. *The Annals of Statistics*, pages 417–421, 1978.
- [7] Kacper P Chwialkowski, Aaditya Ramdas, Dino Sejdinovic, and Arthur Gretton. Fast two-sample testing with analytic representations of probability measures. In *Advances in Neural Information Processing Systems*, pages 1981–1989, 2015.
- [8] Barbara Deschler and Michael Lübbert. Acute myeloid leukemia: epidemiology and etiology. *Cancer*, 107(9):2099–2107, 2006.
- [9] TW Epps and Kenneth J Singleton. An omnibus test for the two-sample problem using the empirical characteristic function. *Journal of Statistical Computation and Simulation*, 26(3-4):177–203, 1986.
- [10] V Alba Fernández, MD Jiménez Gamero, and J Muñoz García. A test for the two-sample problem based on empirical characteristic functions. *Computational statistics & data analysis*, 52(7):3730–3748, 2008.
- [11] Jerome H Friedman and Lawrence C Rafsky. Multivariate generalizations of the wald-wolfowitz and smirnov two-sample tests. *The Annals of Statistics*, pages 697–717, 1979.
- [12] Arthur Gretton, Karsten M Borgwardt, Malte J Rasch, Bernhard Schölkopf, and Alexander Smola. A kernel two-sample test. *Journal of Machine Learning Research*, 13(Mar):723–773, 2012.
- [13] Peter Hall and Nader Tajvidi. Permutation tests for equality of distributions in high-dimensional settings. *Biometrika*, 89(2):359–374, 2002.
- [14] Norbert Henze. A multivariate two-sample test based on the number of nearest neighbor type coincidences. *The Annals of Statistics*, pages 772–783, 1988.
- [15] James J Higgins. Introduction to modern nonparametric statistics. 2003.
- [16] A Kolmogorov. Sulla determinazione empirica di una legge di distribuzione. *G. Ist. Ital. Attuari*, 4:83–91, 1933.
- [17] William Leeb and Ronald Coifman. Hölder–lipschitz norms and their duals on spaces with semigroups, with applications to earth mover’s distance. *Journal of Fourier Analysis and Applications*, 22(4):910–953, Aug 2016.

- [18] Anna V Little, Mauro Maggioni, and Lorenzo Rosasco. Multiscale geometric methods for data sets i: Multiscale svd, noise and curvature. *Applied and Computational Harmonic Analysis*, 2016.
- [19] Arkadas Ozakin and Alexander G Gray. Submanifold density estimation. In *Advances in Neural Information Processing Systems*, pages 1375–1382, 2009.
- [20] Aaditya Ramdas, Sashank Jakkam Reddi, Barnabás Póczos, Aarti Singh, and Larry Wasserman. On the decreasing power of kernel and distance based nonparametric hypothesis tests in high dimensions. In *Twenty-Ninth AAAI Conference on Artificial Intelligence*, 2015.
- [21] Paul R Rosenbaum. An exact distribution-free test comparing two multivariate distributions based on adjacency. *Journal of the Royal Statistical Society: Series B (Statistical Methodology)*, 67(4):515–530, 2005.
- [22] Robert J Serfling. Approximation theorems of mathematical statistics, 1981.
- [23] Sameer Shirdhonkar and David W Jacobs. Approximate earth mover’s distance in linear time. In *Computer Vision and Pattern Recognition, 2008. CVPR 2008. IEEE Conference on*, pages 1–8. IEEE, 2008.
- [24] Nickolay Smirnov. Table for estimating the goodness of fit of empirical distributions. *The annals of mathematical statistics*, 19(2):279–281, 1948.
- [25] Franco Woolfe, Edo Liberty, Vladimir Rokhlin, and Mark Tygert. A fast randomized algorithm for the approximation of matrices. *Applied and Computational Harmonic Analysis*, 25(3):335–366, 2008.
- [26] Ji Zhao and Deyu Meng. Fastmmd: Ensemble of circular discrepancy for efficient two-sample test. *Neural computation*, 2015.

## A Proofs in Section 3

### A.1 Proof of Proposition 3.3

*Proof of Proposition 3.3.* We first verify the positive semi-definiteness of  $\tilde{k}$ : for any  $f$  so that  $\int f(x)^2 p(x) dx < \infty$ , by definition,

$$\int \int \tilde{k}(x, y) f(x) f(y) p(x) p(y) dx dy = \dots = \int \int k(x, y) \tilde{f}(x) \tilde{f}(y) dx dy,$$

the derivation of which omitted, where  $\tilde{f}(x) = \int (p(u)p(x)f(x) - p(x)p(u)f(u)) du$ . The quantity is non-negative by that  $k$  is PSD. Assumption 1 and uniform boundedness of  $k(x, y)$  implies boundedness of  $k_p(x)$  and the constant  $k_{pp}$ , which leads to (1). (2) follows from the continuity of  $k$ . The square integrability of  $\tilde{k}$  then follows from boundedness of  $k$ , which makes the operator Hilbert-Schmidt with  $\sum_k \tilde{\lambda}_k^2 \leq 16$ . Meanwhile,  $\sum_k \tilde{\lambda}_k = \int \tilde{k}(x, x) p(x) dx \leq 4$  by (1) which proves that the operator is in trace class. Mercer’s Theorem applies to give the spectral expansion and the relevant properties, and  $\int \tilde{\psi}_k(x) p(x) dx = 0$  is by

the centering so that  $\int \tilde{k}(x, y)p(y)dy = 0$  for all  $x$ . This proves (3). Finally, by the uniform convergence of Eqn. (20),  $4 \geq \int \tilde{k}(x, x)q(x)dx = \sum_k \tilde{\lambda}_k \int \tilde{\psi}_k(y)^2 q(y)dy$ , which proves (4).  $\square$

## A.2 Proof of Theorem 3.4

**Lemma A.1** (Replacement lemma). *Let  $\nu_k$  be a sequence of positive number so that  $\sum_k \nu_k < \infty$ . Let  $G_{k,n}$  be an array of random variables,  $k = 1, 2, \dots$ ,  $n = 1, 2, \dots$ , s.t. for each  $n$ ,*

$$\mathbb{E}G_{kn} = 0, \forall(k, n), \quad \mathbb{E}G_{kn}G_{ln} = \Sigma_{kl}^{(n)}, \forall(k, n),$$

where  $\Sigma_{kk}^{(n)} < \infty$ . Furthermore, as  $n \rightarrow \infty$ ,

(i)  $\Sigma_{kl}^{(n)} \rightarrow \Sigma_{kl}$ , and for any finite  $K$ ,  $(G_{kn})_{1 \leq k \leq K} \xrightarrow{d} (G_k)_{1 \leq k \leq K}$  where  $(G_k)_{1 \leq k \leq K} \sim \mathcal{N}(0, \{\Sigma_{kl}\}_{1 \leq k \leq K, 1 \leq l \leq K})$ .

(ii) There exists  $B_1 > 0$  s.t.

$$\sum_k \nu_k \Sigma_{kk}^{(n)} < B_1, \forall n$$

and the convergence is uniform in  $n$ .

Meanwhile, let  $\alpha_{kn}$ ,  $\beta_{kn}$ ,  $\gamma_{kn}$  be three double arrays satisfying that

(iii)  $\alpha_{kn} \geq 0$ ,  $|\gamma_{kn}| \leq 1$ ; as  $n \rightarrow \infty$ ,

$$\alpha_{kn} \rightarrow \alpha_k, \quad \beta_{kn} \rightarrow \beta_k, \quad \gamma_{kn} \rightarrow \gamma_k;$$

(iv) There exist  $B_2, B_3 > 0$  s.t.

$$\sum_k \nu_k \alpha_{kn} < B_2, \quad \sum_k \nu_k \beta_{kn}^2 < B_3,$$

for all  $n$ , and the convergence is uniform in  $n$ .

Then, as  $n \rightarrow \infty$ , the random variable

$$U_n = \sum_k \nu_k (\alpha_{k,n} + \beta_{k,n} G_{kn} + \gamma_{k,n} G_{kn}^2), \tag{31}$$

converges in distribution to  $U$  defined as

$$U = \sum_k \nu_k (\alpha_k + \beta_k G_k + \gamma_k G_k^2), \tag{32}$$

where  $U$  has finite mean and variance.

*Proof.* Firstly, we verify that  $U$  is well-defined and has finite variance: notice that (ii) implies that  $\sum_k \nu_k \Sigma_{kk} < B_1$ , (iii) implies that  $\alpha_k \geq 0$ ,  $|\gamma_k| \leq 1$ , and (iv) implies that  $\sum_k \nu_k \alpha_k \leq B_2$  and  $\sum_k \nu_k \beta_k^2 \leq B_3$ .

For finite  $K$ , we define the truncated  $U_K$  as taking the summation from 1 to  $K$  in Eqn. (32). Then

$$|U - U_K| \leq \sum_{k>K} \nu_k \alpha_k + \sum_{k>K} \nu_k |\beta_k| |G_k| + \sum_{k>K} \nu_k G_k^2,$$

and thus

$$\mathbb{E}|U - U_K| \rightarrow 0, \quad \text{as } K \rightarrow \infty, \quad (33)$$

due to the summability of  $\sum_k \nu_k \alpha_k$ ,  $\sum_k \nu_k \beta_k^2$  and  $\sum_k \nu_k \Sigma_{kk}$  (the 2nd term is bounded by Cauchy-Schwarz). Thus  $U_K \rightarrow U$  with probability one, and  $\mathbb{E}|U| < \infty$ . Furtherly,

$$\mathbb{E}(U - \mathbb{E}U)^2 = \mathbb{E}\left(\sum_k \nu_k \gamma_k (G_k^2 - 1)\right)^2 \leq \sum_k \nu_k \sum_k \nu_k \mathbb{E}(G_k^2 - 1)^2 < \infty$$

by that  $\mathbb{E}G_k^4$  is finite. This verifies that  $U$  has finite mean and variance. Actually, by martingale convergence theorem one can show that  $U_K \rightarrow U$  a.s.

Secondly, using a similar argument, defining  $U_{n,K}$  to be the truncated  $U_n$  in Eqn. (31), one can show that

$$\mathbb{E}|U_n - U_{n,K}| \rightarrow 0 \quad \text{as } K \rightarrow \infty \text{ uniformly in } n, \quad (34)$$

by that  $\sum_{k>K} \nu_k \alpha_{kn}$ ,  $\sum_{k>K} \nu_k \beta_{kn}^2$  and  $\sum_{k>K} \nu_k \Sigma_{kk}^{(n)}$  all converges to zero uniformly in  $n$ , which is assumed in condition (ii) and (iv).

Now we come to prove  $U_n \xrightarrow{d} U$ . By Levy's Continuity Theorem, it suffice to show the pointwise convergence of the characteristic function, namely

$$\mathbb{E}e^{itU_n} - \mathbb{E}e^{itU} \rightarrow 0, \quad \forall t.$$

Using the truncation of  $k$  up to  $K$ , we have that

$$\begin{aligned} |\mathbb{E}(e^{itU_n} - e^{itU})| &\leq \mathbb{E}|e^{itU_n} - e^{itU_{n,K}}| + \mathbb{E}|e^{itU_{n,K}} - e^{itU_K}| + \mathbb{E}|e^{itU_K} - e^{itU}| \\ &\leq \mathbb{E}|t||U_n - U_{n,K}| + \mathbb{E}|e^{itU_{n,K}} - e^{itU_K}| + \mathbb{E}|t||U_K - U|. \end{aligned} \quad (35)$$

By Eqn. (33) and (34), for any  $\varepsilon > 0$ , and any  $t$ , we can choose sufficiently large  $K$  s.t. the first and the third term are both less than  $\frac{\varepsilon}{3}$  for any  $n$ . To show that the second term can be made small, we introduce

$$\bar{U}_{n,K} = \sum_{k=1}^K \nu_k (\alpha_k + \beta_k G_{kn} + \gamma_k G_{kn}^2),$$

and by that  $(G_{kn})_{1 \leq k \leq K} \xrightarrow{d} (G_k)_{1 \leq k \leq K}$  (condition (i)),  $\bar{U}_{n,K} \xrightarrow{d} U_K$ . Meanwhile,

$$|U_{n,K} - \bar{U}_{n,K}| \leq \sum_{k=1}^K \nu_k \{|\alpha_{kn} - \alpha_k| + |\beta_{kn} - \beta_k| |G_{kn}| + |\gamma_{kn} - \gamma_k| G_{kn}^2\}.$$

Since  $K$  is finite, and  $\mathbb{E}G_{kn}^2 = \Sigma_{kk}^{(n)}$  is uniformly bounded as  $n$  increases for each  $k$ , we have that  $\mathbb{E}|U_{n,K} - \bar{U}_{n,K}| \rightarrow 0$  as  $n \rightarrow \infty$ , by the convergence of  $\alpha_{kn}$ ,  $\beta_{kn}$  and  $\gamma_{kn}$ . Thus the second term can be bounded by

$$\begin{aligned} \mathbb{E}|e^{itU_{n,K}} - e^{itU_K}| &\leq \mathbb{E}|e^{itU_{n,K}} - e^{it\bar{U}_{n,K}}| + \mathbb{E}|e^{it\bar{U}_{n,K}} - e^{itU_K}| \\ &\leq \mathbb{E}|t||U_{n,K} - \bar{U}_{n,K}| + \mathbb{E}|e^{it\bar{U}_{n,K}} - e^{itU_K}| := \text{(I)} + \text{(II)}, \end{aligned} \quad (36)$$

where (I) can be made smaller than  $\frac{\varepsilon}{6}$  for large  $n$  ( $t$  is fixed and  $\mathbb{E}|U_{n,K} - \bar{U}_{n,K}| \rightarrow 0$ ), and (II) can be made smaller than  $\frac{\varepsilon}{6}$  as a result of  $\bar{U}_{n,K} \xrightarrow{d} U_K$  which implies convergence of characteristic function. Putting together, the l.h.s. of Eqn. (35) can be made smaller than  $\frac{\varepsilon}{3} + \frac{\varepsilon}{3} + \frac{\varepsilon}{3} = \varepsilon$  for large  $n$ , which proves the claim.  $\square$

*Proof of Theorem 3.4 (continued).* To apply Lemma A.1, we set  $\nu_k = \tilde{\lambda}_k$ , and the summability follows (3) of Proposition 3.3; we set  $G_{kn} = \frac{1}{\sqrt{\rho_{1,n}}}\hat{h}_k - \frac{1}{\sqrt{\rho_{2,n}}}\hat{g}_k$ , then  $\mathbb{E}G_{kn} = 0$  by definition, and

$$\begin{aligned} \Sigma_{kl}^{(n)} &= \mathbb{E}G_{kn}G_{ln} \\ &= \mathbb{E}\frac{1}{\rho_{1,n}}\hat{h}_k\hat{h}_l + \mathbb{E}\frac{1}{\rho_{2,n}}\hat{g}_k\hat{g}_l \\ &= \frac{1}{\rho_{1,n}}\delta_{kl} + \frac{1}{\rho_{2,n}}S_{kl}^{(n)}, \end{aligned}$$

where, recalling that  $c_k = \int \tilde{\psi}_k(y)q_1(y)dy$ ,

$$\begin{aligned} S_{kl}^{(n)} &= \int \tilde{\psi}_k(y)\tilde{\psi}_l(y)(p + \tau g)(y)dy - \tilde{v}_k\tilde{v}_l \\ &= (1 - \tau)\delta_{kl} + \tau \int \tilde{\psi}_k(y)\tilde{\psi}_l(y)q_1(y)dy - \tau^2 c_k c_l. \end{aligned} \quad (37)$$

By that  $\rho_{1,n} \rightarrow \rho_1 > 0$  and  $\rho_{2,n} \rightarrow \rho_2 > 0$ , both  $\frac{1}{\rho_{1,n}}$  and  $\frac{1}{\rho_{2,n}}$  are uniformly bounded, so  $\Sigma_{kl}^{(n)}$  are bounded for each  $(k, l)$ . We now verify condition (i) and (ii) in Lemma A.1:

Condition (i): In case (1) and (2),  $\tau \rightarrow 0$ , thus  $S_{kl}^{(n)} \rightarrow \delta_{kl}$  and then  $\Sigma_{kl}^{(n)} \rightarrow \Sigma_{kl} = (\frac{1}{\rho_1} + \frac{1}{\rho_2})\delta_{kl}$ . In case (3)  $\tau \equiv 1$ , thus  $S_{kl}^{(n)} \equiv S_{kl}$  and then  $\Sigma_{kl}^{(n)} \rightarrow \Sigma_{kl} = \frac{1}{\rho_1}\delta_{kl} + \frac{1}{\rho_2}S_{kl}$ . As for the limiting distribution of  $(G_{kn})_{1 \leq k \leq K}$  for any finite  $K$ , we know that  $(\hat{h}_k)_{1 \leq k \leq K} \xrightarrow{d} \mathcal{N}(0, I_K)$ , and  $(\hat{g}_k)_{1 \leq k \leq K} \xrightarrow{d} \mathcal{N}(0, \{S_{kl}\}_{1 \leq k, l \leq K})$  by Lindeberg-Levy CLT (Theorem 1.9.1 B in [22], extended to the case where the covariance matrix converges to a non-degenerate limit by Slutsky Theorem). By definition of  $G_{kn}$  and that  $(\hat{h}_k)_{1 \leq k \leq K}$  and  $(\hat{g}_k)_{1 \leq k \leq K}$  are independent,  $(G_{kn})_{1 \leq k \leq K} \xrightarrow{d} \mathcal{N}(0, \{\Sigma_{kl}\}_{1 \leq k, l \leq K})$  where  $\rho_{1,n}$  ( $\rho_{2,n}$ ) is replaced by  $\rho_1$  ( $\rho_2$ ) by Slutsky Theorem. The argument applies to all the three cases.

Condition (ii):  $\Sigma_{kk}^{(n)} = \frac{1}{\rho_{1,n}} + \frac{1}{\rho_{2,n}}S_{kk}^{(n)} \leq c_1 + c_2S_{kk}^{(n)}$  for some absolute positive constant  $c_1$  and  $c_2$ . Meanwhile, by Eqn. (37),  $S_{kk}^{(n)} = (1 - \tau) + \tau \int \tilde{\psi}_k(y)^2 q_1(y)dy - \tau^2 c_k^2 \leq 1 + \int \tilde{\psi}_k(y)^2 q_1(y)dy$ , thus

$$\sum_k \tilde{\lambda}_k \Sigma_{kk}^{(n)} \leq \sum_k \tilde{\lambda}_k (c_1 + c_2 (1 + \int \tilde{\psi}_k(y)^2 q_1(y)dy)) < \infty,$$

thanks to that  $\sum_k \tilde{\lambda}_k < \infty$  and that  $\sum_k \tilde{\lambda}_k \int \tilde{\psi}_k(y)^2 q_1(y) dy < \infty$  ((4) of Proposition 3.3), and the convergence is uniform in  $n$ .

We now consider the three scenarios respectively:

(1) Let  $U_n = nT_n$ , by Eqn. (25) we have

$$\alpha_{k,n} = (-\tau\sqrt{nc_k})^2 \rightarrow a^2 c_k^2, \quad \beta_{k,n} = -2\tau\sqrt{nc_k} \rightarrow -2ac_k, \quad \gamma_{k,n} = 1,$$

thus (iii) holds. Condition (iv) can be verified by that  $\sum_k \tilde{\lambda}_k c_k^2 < \infty$  (upper bounded by  $\leq \sum_k \tilde{\lambda}_k \int \tilde{\psi}_k(y)^2 q_1(y) dy$ ). As analyzed above,  $\Sigma_{kl}^{(n)} \rightarrow \Sigma_{kl} = (\frac{1}{\rho_1} + \frac{1}{\rho_2})\delta_{kl}$ , and condition (i) and (ii) hold, thus Lemma A.1 applies to give that

$$U_n \xrightarrow{d} U = \sum_k \tilde{\lambda}_k (a^2 c_k^2 - 2ac_k G_k + G_k^2) = \sum_k \tilde{\lambda}_k (-ac_k + G_k)^2, \quad G_k \sim \mathcal{N}\left(0, \frac{1}{\rho_1} + \frac{1}{\rho_2}\right) \text{ i.i.d.}$$

as claimed in the theorem.

(2) Let  $U_n$  be the l.h.s. of the statement, then

$$\alpha_{k,n} = 0, \quad \beta_{k,n} = -2c_k, \quad \gamma_{k,n} = n^{-\delta} \rightarrow 0,$$

and condition (iii) and (iv) hold. Same as in (1),  $\Sigma_{kl} = (\frac{1}{\rho_1} + \frac{1}{\rho_2})\delta_{kl}$  and (i) and (ii) hold, thus Lemma A.1 gives that

$$U_n \xrightarrow{d} U = \sum_k \tilde{\lambda}_k (-2c_k) G_k, \quad G_k \sim \mathcal{N}\left(0, \frac{1}{\rho_1} + \frac{1}{\rho_2}\right) \text{ i.i.d.}$$

By the summability of  $\tilde{\lambda}_k$ ,  $U$  is in same distribution as  $\mathcal{N}(0, \sigma_{(2)}^2)$  as defined in the theorem.

(3) Similar to (2), let  $U_n$  be the l.h.s. of the statement, then  $\alpha_{k,n}$ ,  $\beta_{k,n}$ ,  $\gamma_{k,n}$  are same as in (2) where  $\delta = \frac{1}{2}$ , so they have the same limit, and (iii) and (iv) hold. As analyzed above,  $\Sigma_{kl}^{(n)} \rightarrow \Sigma_{kl} = \frac{1}{\rho_1} \delta_{kl} + \frac{1}{\rho_2} S_{kl}$ , and (i) and (ii) hold. Thus Lemma A.1 gives that  $U_n \xrightarrow{d} U = \sum_k \tilde{\lambda}_k (-2c_k) G_k$  where  $G_k$  has covariance  $\Sigma_{kl}$ . By the summability of  $\tilde{\lambda}_k$ ,  $U$  is in same distribution as  $\mathcal{N}(0, \sigma_{(3)}^2)$ , where  $\sigma_{(3)}^2 = 4 \sum_{kl} \tilde{\lambda}_k \tilde{\lambda}_l c_k c_l \Sigma_{kl}$  which equals the formula claimed in the theorem.  $\square$

## B Proofs of Theorem 3.7 and Theorem 3.9

We first set up certain notations following V-statistics convention which will be used in proofs in this section. They correspond to certain quantities in Section 3 when  $n_1 = n_2$ . We slightly abuse the notation  $n$  to be  $n = n_1 = n_2$  in this case. Let  $z = (x, y)$  which is distributed as  $p \times q$ , and notice that the statistic  $T_n$  can be written as

$$T_n = \frac{1}{n^2} \sum_{i,i'} h(z_i, z_{i'}), \quad z_i = (x_i, y_i),$$

where

$$h(z, z') = \tilde{k}(x, x') + \tilde{k}(y, y') - \tilde{k}(x, y') - \tilde{k}(y, x').$$

By Eqn. (20), defining  $\tilde{\psi}_k(z) := \tilde{\psi}_k(x) - \tilde{\psi}_k(y)$ , we have

$$h(z, z') = \sum_k \tilde{\lambda}_k \tilde{\psi}_k(z) \tilde{\psi}_k(z').$$

We also define

$$h_1(z) := \mathbb{E}_{z'} h(z, z'), \quad h_0 := \mathbb{E}_z h_1(z),$$

recalling that  $\tilde{v}_k = \mathbb{E}_{x \sim p} \tilde{\psi}_k(x) - \mathbb{E}_{y \sim q} \tilde{\psi}_k(y) = \mathbb{E}_z \tilde{\psi}_k(z)$ , then

$$h_1(z) = \sum_k \tilde{\lambda}_k \tilde{v}_k \tilde{\psi}_k(z), \quad h_0 = \sum_k \tilde{\lambda}_k \tilde{v}_k^2, \quad (38)$$

and one can verify that  $h_1(z) = \tilde{k}_1(x, y)$  defined as in Corollary 3.6, and  $h_0 = T$ . Finally, we define  $C_1 := \text{Var}_z(h_1(z))$ , same as in Theorem 3.7. Under Assumption 2, when  $q \neq p$  both  $h_0$  and  $C_1$  are strictly positive, due to that  $\tilde{\lambda}_k > 0$  by definition and there exists some  $k$  so that  $\tilde{v}_k \neq 0$  by assumption.

## B.1 Proof of Theorem 3.7

*Proof of Thm. 3.7.* The proof is by comparing  $T_n$ , the V-statistics, to the associated U-statistics (Lemma B.3), of the latter a Berry-Esseen type result was previously established in [6]:

$$\sup_{x \in \mathbb{R}} \left| \Pr \left[ \frac{\sqrt{n}(T_n - h_0)}{2\sqrt{C_1}} \leq x \right] - \Phi(x) \right| \leq c \frac{\mathbb{E}|h(z, z')|^3}{C_1^{3/2}} n^{-1/2}, \quad (39)$$

where  $c$  is an absolute constant. We also need the following lemma, the proof being elementary and omitted:

**Lemma B.1.** *Suppose that  $\{\xi_n\}_n$  and  $\{\eta_n\}_n$  are two sequence of random variables, and  $a_n$  a sequence of positive numbers,  $a_n \rightarrow 0$  as  $n \rightarrow \infty$ , then*

$$\sup_{x \in \mathbb{R}} |\Pr[\xi_n \leq x] - \Phi(x)| \leq \sup_{x \in \mathbb{R}} |\Pr[\eta_n \leq x] - \Phi(x)| + \Pr[|\xi_n - \eta_n| > a_n] + ca_n, \quad (40)$$

where  $c$  is an absolute constant.

The claim in Thm. 3.7, with  $T_n = V_n$ , follows from applying Lemma B.1 together with Lemma B.3, with  $\xi_n = \frac{\sqrt{n}(V_n - h_0)}{2\sqrt{C_1}}$ ,  $\eta_n = \frac{\sqrt{n}(U_n - h_0)}{2\sqrt{C_1}}$ , and  $a_n = \frac{B}{2\sqrt{C_1}\sqrt{n}}$  where  $B = 2|h_0 - \mathbb{E}h(z, z)|$  as required by Lemma B.3. The first and third term in Eqn. (40) are of order  $O_h(n^{-1/2})$ , and the second term of  $O_h(n^{-1})$ .  $\square$

**Remark B.2.** *The constant in front of  $n^{-1/2}$  is not precisely the same as in the Berry-Esseen bound due to using Chebychev bounds to compare the V-statistics to U-statistics, i.e. Lemma B.3.*

## B.2 A lemma to compare V-statistics to U-statistics

The following lemma compares the V-statistics to the associated U-statistics, and shows that in terms of limit distribution the two are identical as long as the scale is larger than  $O(n^{-1})$ . The bound is equally applicable under  $p = q$  and  $p \neq q$ . The lemma is almost the same as Lemma 6.3.2.C in [22]. The difference is that by assuming square-integrability of  $h(z, z)$  we end up getting an explicit  $O(n^{-1})$  bound, though the  $o(n^{-1/2})$  bound as in [22] leads to same bound for the Berry-Esseen rate. We reproduce the result for completeness.

**Lemma B.3** (Lemma 6.3.2.C, [22] (modified)). *Let  $z_1, \dots, z_n$  i.i.d.  $\sim dF(z)$  some distribution, and  $h(z, z')$  be a symmetric function, with*

$$\mathbb{E}h(z, z')^2 = \int \int h(z, z')^2 dF(z) dF(z'), \quad \mathbb{E}h(z, z)^2 = \int h(z, z)^2 dF(z) < \infty.$$

Consider the V-statistics and the associated U-statistics

$$V_n = \frac{1}{n^2} \sum_{i, i'=1}^n h(z_i, z_{i'}), \quad U_n = \frac{1}{n(n-1)} \sum_{i \neq i'} h(z_i, z_{i'}).$$

We have that, whenever  $B \geq 2|\mathbb{E}h(z, z') - \mathbb{E}h(z, z)|$ ,

$$\Pr[|U_n - V_n| > \frac{B}{n}] \leq \frac{1}{B^2} O_h(n^{-1}),$$

where the subscript  $h$  denotes that in the asymptotic bound the constant depends on  $h$ .

*Proof.* By construction,

$$U_n - V_n = \frac{1}{n}(U_n - W_n), \quad W_n := \frac{1}{n} \sum_i h(z_i, z_i).$$

We firstly control the concentration of  $W_n$  at  $\mathbb{E}W_n$  by Chebyshev:  $\mathbb{E}W_n = \mathbb{E}h(z, z) := b_0$ , and let  $\text{Var}_z(h(z, z)) = b_2 < \infty$ , we have that

$$\Pr[|W_n - b_0| > t] \leq \frac{1}{t^2} \frac{b_2}{n}, \quad \forall t > 0.$$

Similarly, for  $U_n$ ,  $\mathbb{E}U_n = \mathbb{E}h(z, z') = h_0$ ,  $\text{Var}_{z, z'}(h(z, z')) = C_2 < \infty$ ,  $\text{Var}_z(\mathbb{E}_{z'} h(z, z')) = C_1 \leq C_2 < \infty$ . The computation of the 2nd moment, using the fact that  $\mathbb{E}h(z_1, z_2)h(z_1, z_3) = C_1$ , gives that

$$\mathbb{E}(U_n - \mathbb{E}h_0)^2 \leq \frac{n(n-1)(n-2)C_1 + n^2 C_2}{n^2(n-1)^2} \leq O_h(n^{-1}). \quad (41)$$

Thus

$$\Pr[|U_n - h_0| > t] \leq \frac{1}{t^2} O_h(n^{-1}), \quad \forall t > 0.$$

Putting together, when  $\frac{B}{2} \geq |h_0 - b_0|$ ,

$$\begin{aligned}
\Pr[|U_n - V_n| > \frac{B}{n}] &= \Pr[|U_n - W_n| > B] \\
&= \Pr[|(U_n - h_0) - (W_n - b_0) + (h_0 - b_0)| > B] \\
&\leq \Pr[|U_n - h_0| > \frac{B}{4}] + \Pr[|W_n - b_0| > \frac{B}{4}] \\
&\leq \frac{1}{(B/4)^2} \frac{b_2}{n} + \frac{1}{(B/4)^2} O_h(n^{-1})
\end{aligned}$$

which proves the claim.  $\square$

### B.3 A Chebyshev bound for $nT_n$ under $\mathcal{H}_0$

**Lemma B.4.** *Notations as above, under  $\mathcal{H}_0$ , whenever  $a > 4b_0$ ,  $b_0 = \mathbb{E}h(z, z) = 2 \sum_k \lambda_k$ ,*

$$\Pr[nT_n > 2b_0 + t] \leq \frac{C_2}{t^2} + \frac{b_2}{b_0^2} \frac{1}{n}.$$

where  $C_2 = \text{Var}_{z, z'}(h(z, z')) = 4 \sum_k \lambda_k^2$ ,  $b_2 = \text{Var}_z(h(z, z))$ .

*Proof.* Write  $nT_n = U'_n + W_n$ , where  $U'_n = \frac{1}{n} \sum_{i \neq i'} h(z_i, z_{i'})$ , and  $W_n$  is as in the proof of Lemma B.3, so we have that

$$\Pr[|W_n - b_0| > t] \leq \frac{1}{t^2} \frac{b_2}{n}, \quad \forall t > 0.$$

Following the same calculation as in Eqn. (41), we have that  $\mathbb{E}(U'_n)^2 \leq C_2$  (notice that  $C_1$  vanishes in this case, and normalization is  $1/n$  instead of  $1/(n-1)$  as in the U-statistics). This gives that

$$\Pr[|U'_n| > t] \leq \frac{C_2}{t^2}, \quad \forall t > 0.$$

The claim follows from that  $\Pr[nT_n > 2b_0 + t] = \Pr[U'_n + b_0 + (W_n - b_0) > 2b_0 + t] \leq \Pr[U'_n > t] + \Pr[W_n - b_0 > b_0]$  and the combination of the two Chebyshev bounds.  $\square$

### B.4 Proof of Theorem 3.9

*Proof of Theorem 3.9.* Let  $h_1^{(1)}(z) := \mathbb{E}_{z'}[h(z, z') | \mathcal{H}_1]$ . As explained in the beginning of this section, Assumption 2 implies that both  $C_1^{(1)} = \text{Var}_z(h_1^{(1)}(z))$  and  $h_0^{(1)} := \mathbb{E}[h(z, z') | \mathcal{H}_1]$  are strictly positive. Theorem 3.7 applies to give that

$$\Pr[T_n \leq h_0^{(1)} - \frac{2\sqrt{C_1^{(1)}}}{\sqrt{n}} x | \mathcal{H}_1] \leq \Phi(-x) + O_h(n^{-1/2}), \quad \forall x > 0. \quad (42)$$

Recall that the threshold  $t_\alpha$  equals  $\inf_t \{t, \Pr[T_n > t | \mathcal{H}_0] \leq \alpha\}$ , and, by Lemma B.4, it can be written as

$$t_\alpha = \frac{2b_0^{(0)} + t'_\alpha}{n}, \quad (43)$$

where  $t'_\alpha$  can take the smallest (positive) value so that

$$\frac{C_2^{(0)}}{(t'_\alpha)^2} + \frac{b_2^{(0)}}{(b_0^{(0)})^2} \frac{1}{n} \leq \alpha,$$

with  $b_0^{(0)} = \mathbb{E}[h(z, z) | \mathcal{H}_0] = 2 \sum_k \tilde{\lambda}_k$ ,  $b_2^{(0)} = \text{Var}_z[h(z, z) | \mathcal{H}_0]$ , and  $C_2^{(0)} = \text{Var}_{z, z'}[h(z, z') | \mathcal{H}_0] = 4 \sum_k \tilde{\lambda}_k^2$ . Thus, with sufficiently large  $n$  (e.g.  $n > \frac{b_2^{(0)}}{(b_0^{(0)})^2} \frac{2}{\alpha}$ ) the value of  $t'_\alpha \sim \sqrt{C_2^{(0)}/\alpha}$ , which, substituting into Eqn. (43), implies that  $t_\alpha \sim O(n^{-1})$ . Back to Eqn. (42), setting  $h_0^{(1)} - \frac{2\sqrt{C_1^{(1)}}}{\sqrt{n}}x = t_\alpha$  results in the r.h.s. of Eqn. (42) an upper bound of  $1 - \pi_n(\tau)$ , and then

$$x = \frac{\sqrt{n}(h_0^{(1)} - t_\alpha)}{2\sqrt{C_1^{(1)}}} \sim O(\sqrt{n})$$

makes  $\Phi(-x)$  exponentially small and then the r.h.s is dominated by  $O_h(n^{-1/2})$ . Thus we prove that  $1 - \pi_n(\tau) \leq O_h(n^{-1/2})$ .  $\square$